Adhesive Joining of Curved Metal and Composite Structures

by

Christopher Gouldstone

S. B., Aeronautics and Astronautics, Massachusetts Institute of Technology, Cambridge, Massachusetts (2000)

Submitted to the Department of Aeronautics and Astronautics
in partial fulfillment of the requirements for the degree of

MASTER OF SCIENCE IN AERONAUTICS AND ASTRONAUTICS

at the

MASSACHUSETTS INSTITUTE OF TECHNOLOGY

June 2002

Author_____
Department of Aeronautics and Astronautics
May 17, 2002

Certified by_____
S. Mark Spearing
Associate Professor of Aeronautics and Astronautics
Thesis Supervisor

Accepted by_____
Wallace Vander Velde
Professor of Aeronautics and Astronautics
Chair, Committee on Graduate Students

Adhesive Joining of Curved Metal and Composite Structures

by

Christopher Gouldstone

Submitted to the Department of Aeronautics and Astronautics
on May 17, 2002, in partial fulfillment of the
requirements for the degree of
Master of Science in Aeronautics and Astronautics

Abstract

Joining metallic and composite components by adhesive bonding offers comparable performance to metal-metal and composite-composite bonding, but presents unique challenges. Joint design and fabrication methods need to be evaluated to ensure reliable, high-strength bonding. This work evaluates such methods for producing adhesive joints between metal and composite components with curved bonding surfaces. The benefits of adherend surface preparation for such a configuration are quantified experimentally, while thermal effects and plasticity are studied using finite element modeling. Bond strength is shown to increase by 100% through improvements in surface preparation alone.

Composite test specimens were fabricated by joining, either adhesively or mechanically, aluminum discs with graphite-epoxy cylinders. The discs were bonded to the interior surface of the cylinders, or jointed using radially-inserted machine screws. Each specimen was loaded in a servohydraulic testing machine along its longitudinal axis, using a load spreader to apply upward pressure to the aluminum disc, to facilitate extraction of the disc from the cylinder. Specimen failure was seen to be a fracture-dominated process.

Finite element simulations were performed using axisymmetric models of the adhesively-bonded structure, employing thermal and mechanical loads and boundary conditions consistent with the manufacturing procedures and test configurations used. Thermal stresses were introduced by cooling the structure down from a stress-free adhesive cure temperature. The structure was subsequently loaded by a uniform edge displacement of the aluminum. Stress analysis was completed using ABAQUS software, with a refined mesh in and around the bonded region. FRANC2D software was used for fracture analysis of the bond, by initiating an edge crack in the adhesive layer.

Thesis Supervisor: S. Mark Spearing
Title: Associate Professor of Aeronautics and Astronautics

Acknowledgments

This work concludes a healthy stint of six years at the institute, and many of my fondest memories are from my time spent with TELAC. For inviting me to join, and for so much more, I am truly grateful to Prof. Mark Spearing. Over five years he has been my teacher, advisor and my friend. I can safely say I have learnt more from him than from anyone else at MIT.

I am indebted to Will McFarland, Jr. for his guidance and encouragement throughout this work, and to Draper Labs for their financial support. I owe special thanks to Seth Kessler for sharing his vast experience in composite manufacture and testing, particularly while he was trying to graduate. This is not the first project that he has seen me through. His mentorship has aided me greatly and his determination spooks and inspires me.

I would like to extend my gratitude to John Kane, who helped me to ask the right questions, and to Don Weiner, who never tired of them. Thanks to Nick Abercrombie, for all his help during IAP, and to all of the extra pairs of hands who helped with manufacturing. For navigating myself and many others through the rocky shallows of institute requirements, I offer my most sincere appreciation to Marie Stuppard.

Thanks also to Jeremy Gregory, Kevin Turner, Torrey Radcliffe, Dong Jin Shim and Linda Mendenhall from the TELAC office, and to Mark Kepets for always making my problems seem so small.

To Mama and Pops, thank you for providing for my education, and for bustin' heads all the times when education wasn't what I was getting. I owe fourteen tons of gratitude to my brother Roo, who is at once incredible, amazing, and uncanny – a true ABAQUS marvel. I admire my big brother Jim, who first brought the Gouldstones to Boston, where we've all had such good fortune, and equally my little brother Ian, who continues, fearlessly, to blaze new trails all his own.

Most everyone I know has had to endure, usually more than once, the twisted mockings I call my sense of humor. For this I should be thanking everyone over again. No one person, though, has done so with more forbearance than Pimpa Limthongkul (da Pimp, Pizzimp, Pimpa the Clown). Pimpressive, I think.

No acknowledgment I could draft could adequately express what I owe this last person, but if there's one thing she's used to, it's my inadequacy. Thank you, the Shen, for all the sweet things we have shared in four years, and to a lesser extent, the veggies.

Contents

List of Figures

List of Tables

Chapter 1

Introduction

1.1 Motivation

Adhesive joining is an attractive technique for composite structures. Bonded joints are particularly desirable in weight-sensitive, high-reliability applications because they can reduce mass and lower part count.

Metal components are often joined together using mechanical fasteners, such as bolts or rivets. Using fasteners tends to introduce stress concentrations around holes cut for the bolts themselves. In addition, tightened bolts generate compressive loads. While these same effects occur if the components are made of metal or of carbon fibre-reinforced polymer (CFRP) materials, they can in many cases be more problematic with components made of the latter. Under the same loading, an orthotropic laminate containing holes may have amplified stress concentration factors over a isotropic metal structure with holes. The higher stress concentrations increase the likelihood of structural failure.

The ability of the structure to suppress fracture and fatigue can be limited by the cracks near the hole edge. These cracks can arise from damage caused by the machining procedure used to make the hole. The large number of terminated fibres at the hole edge can further weaken the structure.

Many industries are now realizing potential applications where composites would outperform traditional metallic construction materials. While the aerospace industry has ar-

guably been the earliest adopter of composites for weight-saving, the automotive industry is just now beginning to integrate composite components into high-volume production vehicles, to reduce weight and thereby improve fuel economy.

These two industries are notable for their traditional devotion to building their primary structures from a single metallic building material. In aerospace, this has been specific grades of aluminum alloys. In passenger vehicle construction, steel has been used with few exceptions, although aluminum is becoming more popular for performance and luxury cars, and as an engine material.

As composite materials become cheaper and easier to manufacture in large volumes, their uses will continue to grow. However, they will first be integrated with existing metal structures, rather than replacing them altogether. Even today, there are many structural configurations which require joining of metal and composite components for exactly these reasons.

By using adhesives to join these dissimilar adherends, joint performance comparable to metal-to-metal or composite-to-composite bonds is achievable, but there are additional challenges when bonding materials with different properties.

The failure modes of adhesive bonds are several, and distinct from those of mechanically fastened joints. They include adhesive, cohesive and adherend failure. Adhesive failure happens when two different materials disconnect at the interface between them. Cohesive failure is categorized by fracture contained within the adhesive, leaving each bi-material interface intact while severing the connection between the adherends. Adherend failure is described as sufficient damage within one or more of the adherends to bring about overall joint rupture, while the adhesive and bi-material interfaces remain intact. Joint failure may also occur by a combination of adhesive, cohesive and adherend damage.

Adhesive damage is the least desirable cause of failure. When cohesive or adherend failure occurs, it means one or more of the bond components has been loaded to failure, limiting bond strength. Adhesive failure does not occur due to failure of a constituent of the bond, but rather as the result of interfacial failure. Preventing adhesive failure requires careful preparation of adherend surfaces to maximize adhesion between them.

Another concern with adhesive bonding at elevated temperatures is residual stress, which

is locked in when materials with mismatched thermal properties are cooled back down after curing. The presence of these stresses can reduce the maximum applied stress the bond can withstand compared to a similar bond which is stress-free before applied loading.

The applications for bonding flat structural components represent only a small part of the potential for structural bonding, yet the majority of previous work in adhesive bonding of composites uses flat specimens. While these tests can be effective at characterizing bond performance to an extent, they do not address the obstacles that arise when joining structures with more generic geometries. To minimize aerodynamic drag, wetted aerospace structures are, almost without exception, inherently curved. Joining these to internal structural components often occurs at a curved interface, so understanding joining of curved structures is crucial.

When faced with such a variety of significant factors affecting bond performance, materials selection, joint configuration, design and manufacture, manufacturing methods must be evaluated to ensure joint integrity, strength and reliability.

1.2 Objectives

The primary objectives of this work are to evaluate the feasibility of creating high reliability bonds between curved components and the methods available for modeling their behavior. To determine the factors affecting reliable bonding, one goal is to quantify the effect of adherend surface preparation on performance of a cylindrical bond between a composite tube and a metallic plug. The importance of thermal effects and plasticity are studied also to determine the influence of bonding procedures and adhesive selection on joint strength. The structural configuration was to be modeled using a finite element software package to estimate internal stresses and implement various failure criteria. Firstly though, a feasible manufacturing procedure had to be determined in order to realize these goals.

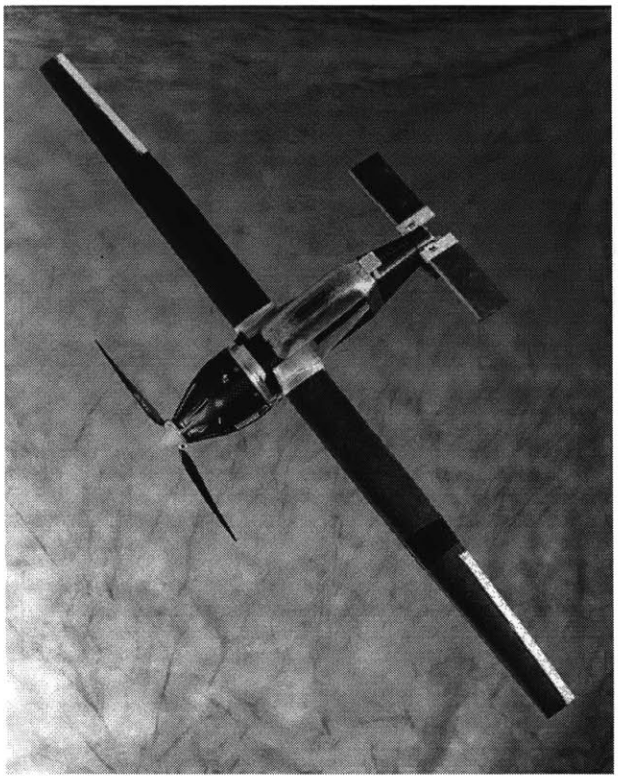

Figure 1-1: W.A.S.P. aircraft, courtesy of Draper Laboratories

1.3 Approach

In pursuit of these goals, a representative structural configuration was selected as the focus of the experimental and analytical work. Having selected a generic geometry, manufacturing procedures for joining components were developed. The procedures were then evaluated empirically by mechanical testing, and analytically through finite element simulations.

The geometry selected was based upon a sub-assembly of the Wide Area Surveillance Projectile ("WASP") which was, at the time, an ongoing project underway at Draper Laboratory in Cambridge, MA. The WASP is a small, unmanned, reconnaisance aircraft, designed to fit inside an artillery shell in its undeployed state, and survive a high-g launch from a 5" gun [8].

In one recent design iteration, shown in Figure 1-1, the aircraft featured an aluminum bulkhead connecting a tubular composite fuselage to the rear with a composite nosecone facing forward. It was intended that one or both of these interfaces be adhesively bonded.

Following selection of this generic geometry, the details of the test specimen geometry

and testing program were determined.

A manufacturing procedure for composite tubes by Kessler [8] was used to make the fuselage components, while the bulkheads were envisioned as aluminum parts with radial symmetry, which were inserted and bonded into the tubes. For strength testing, the specimens were loaded centrally, parallel to the long axis of the tubes.

A set of adhesive systems and temperatures were chosen for bonding the test specimens. Evaluating the influence of assembly tolerance between the metal and composite required different adhesive systems to be used. Different cure temperatures allowed residual thermal stresses to be introduced in certain cases.

Joined specimens were loaded until the aluminum insert was completely extracted from the tube. During extraction, the load and displacement of the testing machine head were recorded, so that salient mechanical behavior could be identified.

1.4 Thesis Outline

This thesis is intended to provide the reader with a clear and concise explanation of the work undertaken. The thesis is structured as follows.

Chapter 1 describes the motivation and objectives of the work. In this chapter a broad outline of the experimental approach can also be found. In Chapter 2 a summary of previous work and its relevance to this project is discussed. Chapter 3 covers the analytical modeling conducted as part of this thesis. Details include model generation and assumptions, material properties used and loads applied. In Chapter 4, the results of these analyses are presented along with a discussion of the failure criteria used. Chapter 5 documents the experimental aspects of the project. Fabrication of test specimens and test hardware is documented, as are all testing procedures. Chapter 6 summarizes the experimental results. The chapter presents test data for ultimate strength, qualitative observations on defects, failure modes and features of failed specimens. Chapter 7 compares experimental data with numerical analysis and attempts to identify sources of disagreement. In the final chapter, Chapter 8, conclusions of the project are presented including recommendations for producing high-reliability joints between dissimilar curved components. This thesis concludes with recommendations for

future work.

Chapter 2

Background

2.1 Adhesive Joining

The benefits of joining with adhesives rather than mechanical fasteners are summarized by Andrews [9]. Stress concentrations that are seen in riveted joints are largely avoided in adhesive joints, because the stresses are distributed over a far greater area. Eliminating stress concentrations improves fatigue life of a joint, and additional material is not required to bolster the joint, as it would be around a bolt hole. Weight savings relative to mechanical fasteners can reach as much as 25%, depending upon the type of loading seen by the structure. Since adhesive bonds are distributed over a large area, the resulting joint is stiffer than a riveted equivalent, which constrains the structure in a far smaller region. Adhesives make possible the joining of delicate or brittle structures which could be damaged by riveting. Graphite-Epoxy composite structures often fit into this category, and tend to sustain damage when holes are machined into them.

While adhesive joints offer considerable performance advantages, other factors often result in bolted joints being favored. Bonding dissimilar components can introduce appreciable thermal stresses. Bonded structures are difficult to inspect and cannot be disassembled. They are also prone to environmental degradation and are sensitive to bonding procedures [10].

In contrast, bolted joint fabrication and inspection are both simple, and do not result

in residual stresses contained within the joint. Bolted joints are relatively insensitive to the environment and enjoy a wider range of applications than adhesives. For metal components of sufficient thickness, a bolted connection is often the more appropriate choice.

2.2 Previous Work

2.2.1 Curved Specimens

The procedure for manufacturing composite tubular specimens used in this project was created by Kessler, as part of a project completed in 2000 to design a high-g tolerant structure for the WASP aircraft [8]. Kessler did some preliminary work on attaching the composite fuselage to the aluminum fore-bulkhead using a cleaning/sanding surface preparation. His joining methods spanned both adhesive bonding and mechanical fastening, but suffered a high rate of adhesive failure, which limited the strength of the bonds to far below that of the adhesive itself. He attributed this type of failure to inadequate surface preparation.

2.2.2 Surface Preparation and Bonding

Adhesive bonding has suffered slow adoption for joining of primary structures. A high rate of bond failures in service (typically of repair patches or minor structural joints) has called the reliability of the adhesives into question [11]. Many agree though that the poor performance of adhesive bonds can be attributed much more to bond design and fabrication procedure than to any intrinsic material property [12]. Adhesive bonding for industrial applications has a shorter history than the use of mechanical fasteners. Over only the last 50 years though, a large body of literature has been published concerning design principles for effective adhesive joining. Analysis methods, structural tests and design guides that are now available are speeding the introduction of adhesive bonding into more critical flight structures, particularly those constructed from composites.

The crucial importance of proper surface treatment for long-term bond strength is highlighted by Davis. Each adherend surface, he states, must be uncontaminated, chemically active and resistant to hydration [11]. The methods for satisfying these criteria vary in their

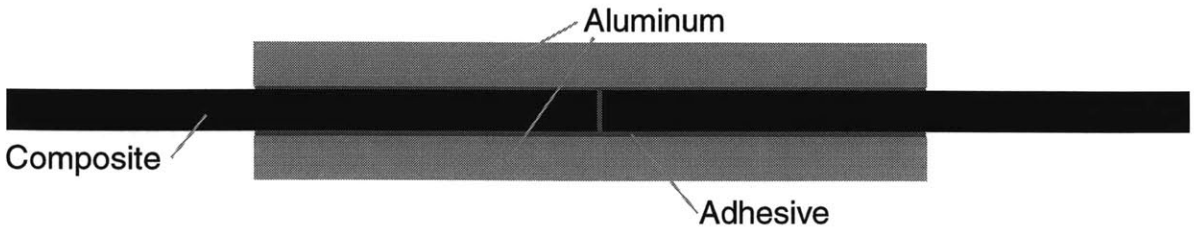

Figure 2-1: Double lap shear specimen

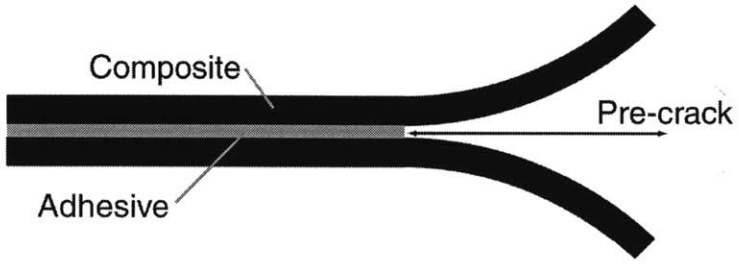

Figure 2-2: Double cantilever beam specimen

applicability to and performance with different materials.

Barbara Huppe completed a research project [2] in June 2001, investigating the effects of surface preparation and manufacturing procedures on the bond strength of metal-composite joints. Double lap shear (DLS) specimens and double cantilever beam (DCB) specimens were fabricated for compliance with ASTM standards for mechanical testing of bonded joints. These test geometries are shown in Figures 2-1 and 2-2.

In order to improve the bonding, Huppe tested many combinations of composite surface preparation and metal surface preparation. The composites were either unprepped, cured with peel-ply instead of release film, or sanded. The aluminum adherends were prepared in a number of different ways. Some were sanded to remove the oxidation layer prior to bonding. Others were primed using BR-127 chemical etchant. Some of the primed components were also grooved to increase their bonding surface area. Still other metal parts were anodized. Of these combinations, Huppe observed the highest strength from sanded composites bonded to primed aluminum.

In addition to surface preparation, Huppe used two different manufacturing methods. In most cases, the adhesive bonding was performed as a secondary bond using previously

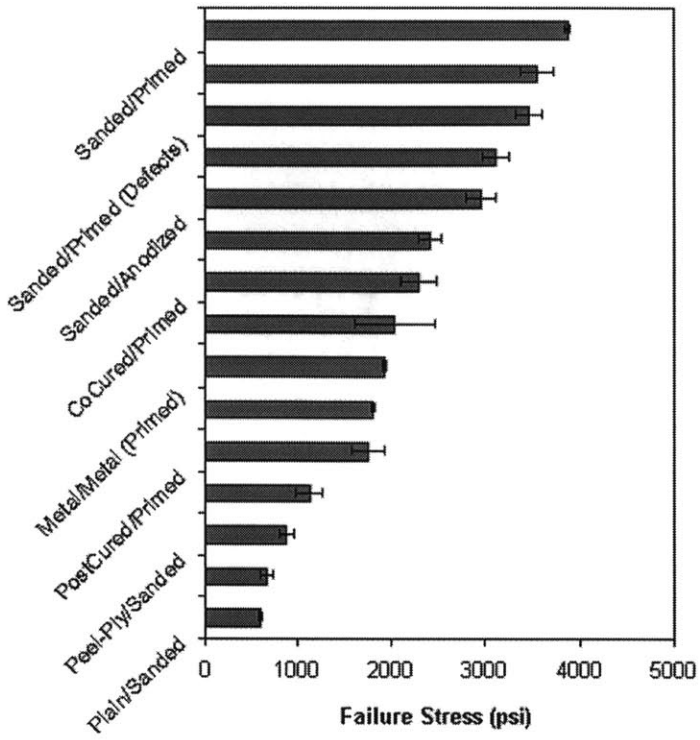

Figure 2-3: Bond strength against specimen preparation [2]

cured graphite-epoxy laminates. In the remaining cases, however, the laminae were co-cured with the adhesives into bonded specimens in a single cure. Using both methods, the bonded sheets were machined into test specimens after joining. While co-curing afforded higher strengths than using unpreparared composites, the co-cured specimens were not as strong as those made with sanded composites in a secondary cure. In addition, the process of cocuring was considered a more difficult manufacturing procedure, despite reducing the number of required cures. A summary of experimental results from Huppe are depicted in Figure 2-3.

The work completed by Huppe provides, in large part, the starting point for this work, which carries on using her conclusions about surface preparations, and seeks to identify complexities encountered in moving from flat coupons to curved components.

A large body of work exists in the fields of composite bonding [13, 14, 4], metal-composite bonding [15, 12, 16, 3, 2, 17-19], and metal-metal bonding [20]. The majority of this work, however, was conducted at the coupon level, using flat specimens assembled into either DLS or DCB samples. Loftus et al questioned the applicability of strength and fatigue data

procured from standard test geometries to more practical geometries [16]. Their specimens bonding small metal attachments to larger composite structures (as seen in race cars) were found to be significantly stronger than supposed using standard tests, with fatigue lives several times greater also.

There is agreement that adhesive bonding has vast potential for joining of composites, and composites with dissimilar materials [21, 11, 19, 12]. In applications where metal components are being replaced with lighter weight composites, the fastening methods also must often be replaced. Spot-welding, commonly used for joining steel automotive structures, is viable neither for aluminum nor composites [22], while adhesives produce stiffer bonds without additional weight. Using mechanical fasteners with composite laminates requires holes to be machined through the laminate, damaging the hole. Van Rijn states "to retain strength an increase in plate thickness by a factor of approximately 3 is required locally." [12]

2.2.3 Thermal Effects

Huppe identified residual thermal stresses as an important issue in bonding of dissimilar components. In addition to the thermal mismatch between the adherends and the adhesive, there is further mismatch between the adherends themselves. This introduces stresses into the structure, and particularly into the bond, which add to the stresses introduced by applied loading, thereby reducing the load-carrying capability of the structure. A closed-form analysis of thermal mismatch and stiffness imbalance in DLS joints was presented by Hart-Smith [23].

Further work in this area [3] was carried out by Watkins and Park in 2001, whose research was focused on determining the scale of the residual thermal stresses Huppe had encountered by varying the temperature difference between curing and testing. As with Huppe, DLS metal-composite specimens were subjected to tension tests using a servohydraulic load frame, but in these tests a thermal chamber was integrated to heat or cool the specimens to the desired temperature.

Watkins and Park estimated the thermal stresses present in the specimens using a thermal model analysed using ABAQUS software. Specimens were loaded to failure at various

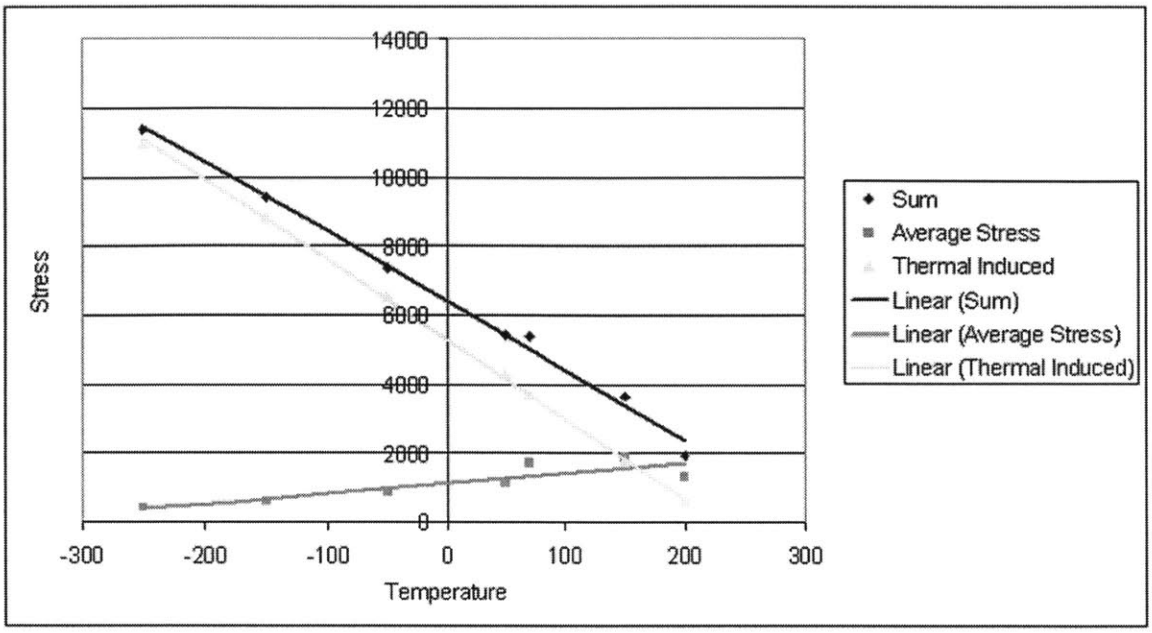

Figure 2-4: Stresses in Al-GrEp DLS specimens [3]

temperatures. The maximum applied stress was superposed with the thermally-induced stress to determine the overall strength of the bond as a function of temperature. They measured approximately 500% greater strength of the bond at -250F than at 200F, with the strength varying quite linearly at temperatures in between. However, the strength benefit at low temperatures could not be realized, because while strength increased with lower temperatures, residual stress grew at an even greater rate. The actual load-carrying capability of the specimens improved with increasing temperature by slightly over 200%. These results are shown in Figure 2-4.

Chapter 3

Finite Element Modeling

3.1 Introduction

This chapter discusses the set of numerical analyses carried out to predict the strength of the bonds between curved adherends that are the focus of this work. Two separate software packages were used to investigate four different failure criteria. The bulk of these analyses, concerned with quantifying stress and strain, proceeded using ABAQUS/CAE. Modeling of the structure for fracture analysis was primarily completed using FRANC2D. Details of the model creation are presented in this chapter. The results of these analyses are summarized in Chapter 4.

3.2 Failure Criteria

Various modes of failure are possible for bonded specimens. An attempt was made to determine the limiting behavior of these specimens by considering a number of failure criteria and using them to estimate specimen strength.

3.2.1 Maximum/Average Shear Stress

ABAQUS/CAE was used to estimate the maximum shear stress observed in the bond as the plug was steadily extracted. The software was also used to determine the mean shear stress

encountered throughout the bond.

3.2.2 Von Mises Yield Criterion

The ABAQUS software returns the Von Mises stress by default in its analyses. The Von Mises stress is calculated from the principal stresses according to:

$$\sigma_{vm}^2 = \frac{1}{2}[(\sigma_{II} - \sigma_{III})^2 + (\sigma_I - \sigma_{III})^2 + (\sigma_I - \sigma_{II})^2] \tag{3.1}$$

The criterion estimates that a material will yield in regions where the Von Mises stress exceeds the yield strength, σ_y:

$$\sigma_{vm} \geq \sigma_y \tag{3.2}$$

3.2.3 Strain Invariant Failure Theory [1]

This criterion proposes that failure of a structure will occur when the first strain invariant, ϵ_1 exceeds some critical value ϵ_c. The first strain invariant is defined as the sum of the principal strains, as expressed by equation 3.3.

$$\epsilon_1 = \epsilon_I + \epsilon_{II} + \epsilon_{III} \tag{3.3}$$

The property ϵ_1, can also be extracted from ABAQUS.

3.2.4 Fracture

Fracture mechanics is based upon the idea that for a crack to propagate, a certain energy per unit area of new crack is required. Assuming an initial pre-crack, one can determine the increase in energy δU required to create new crack area δA. Fast fracture is assumed to occur when the ratio of these quantities, known as the strain energy release rate G, exceeds the critical strain energy release rate G_c, a material parameter governing fracture. Since the energy stored in the structure U depends upon the thermomechanical loading, a critical crack size can be identified for fracture at a given load [24].

In this work the fracture analysis was carried out using FRANC2D software [25].

The stress intensity factor K, a measure relating the geometry and loading, can be determined from equation 3.4.

$$K = \sigma\sqrt{\pi a} \tag{3.4}$$

At the onset of fast fracture, the quantity $\sigma\sqrt{\pi a}$ is a constant, known as the critical stress intensity factor or fracture toughness K_c. By specifying the fracture toughness of the adhesive, K_c $(= \sqrt{EG_c})$, where E is the Young's modulus, the stress at which K exceeds K_c can be determined for a given crack length a. Conversely, the critical crack length at a given stress can be found if K_c is known.

3.3 Stress Analysis

3.3.1 Platform

The majority of the finite element simulation was carried out using ABAQUS/CAE. The models were run on a desktop computer in TELAC running Windows 2000 Professional on dual Pentium 4 processors. Model creation, analysis and results postprocessing all took place within CAE.

3.3.2 Geometry

The model constructed in ABAQUS/CAE is shown in Figure 3-2. The main model was constructed as axisymmetric, which was described by a planar section of the bonded specimen and an axis of revolution. There were three parts to the assembly: a representation of the tube, one of the plug, and a third to model the adhesive. Since the plug is shaped as a disk with a centered hole, its section was constructed as a 0.5" by 1.22" rectangle displaced from the axis by 0.5". Similarly, the tube was constructed as a rectangle measuring 2.5" long by 0.1" wide, while the bond was modeled in a number of ways to fit in the space between the two adherends.

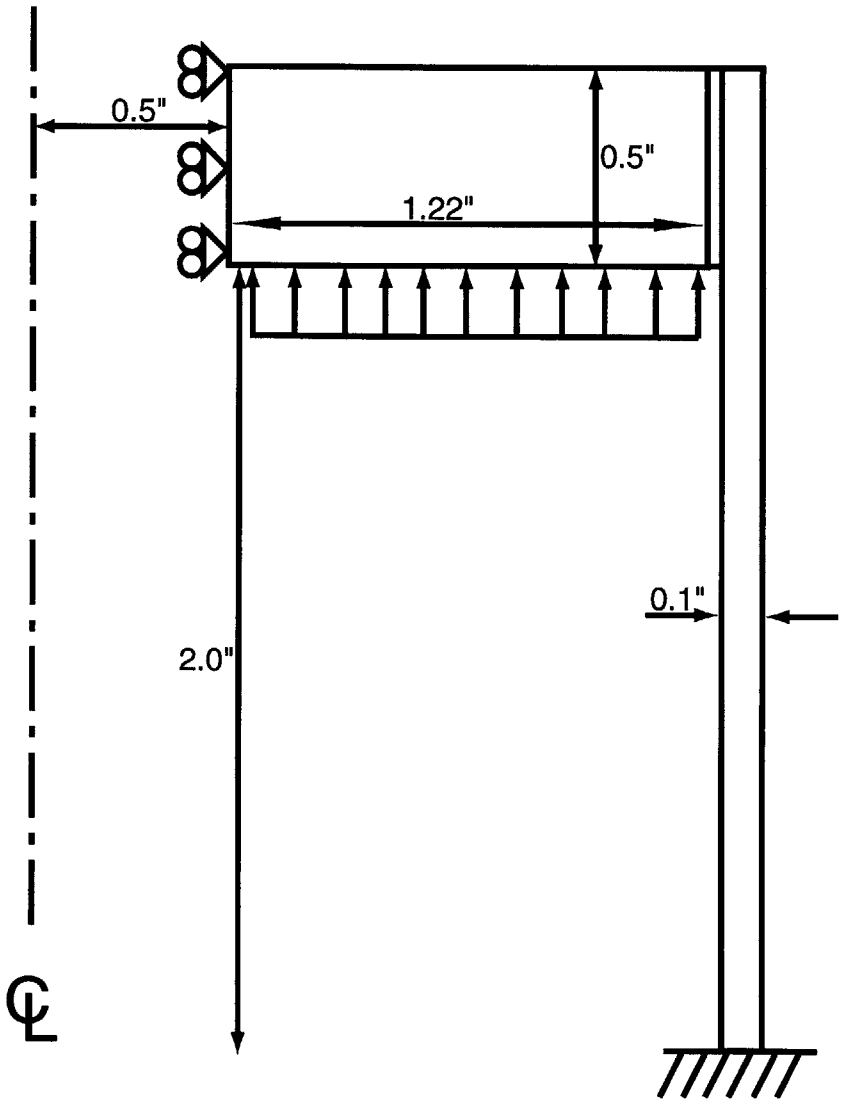

Figure 3-1: Specimen geometry, loads and boundary conditions

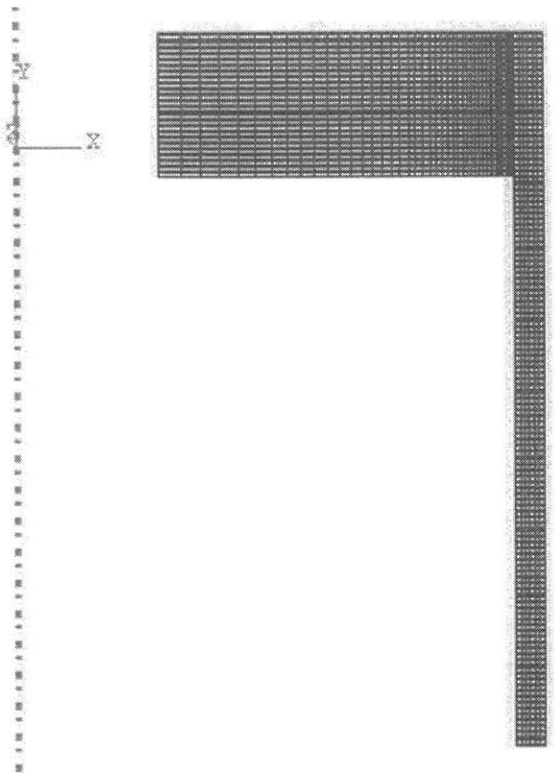

Figure 3-2: Finite element model of bonded specimen

3.3.3 Materials

There are three major material constituents of an assembled specimen. Each of the two adherends is made of a different material and the bond out of a third.

The tubes were made of AS4/3501-6 graphite epoxy 18-ply laminates. The stacking sequence was $[0\pm45]_{3s}$. Since this is a balanced, symmetric layup, the material is characterized as orthotropic, and is described by 9 elastic constants. These constants were determined using Classical Laminated Plate Theory (CLPT) [26] by transforming known properties of a unidirectional ply. The thermal expansion coefficients were derived also from ply properties, by constructing a flat laminate of the same stacking sequence in ABAQUS.

Due to the directionality of the laminate, a material coordinate system had to be specified in CAE. The properties specified in Table 3.2 are consistent with a coordinate system whose 1-direction extends radially outward from the tube axis, which lies collinear with the 2-direction. The 3-direction points circumferentially, lying in the plane of the laminate plies.

The plug insert was made of aluminum 2024-T351 and was modeled as an isotropic

Table 3.1: Material data: Aluminum [5]

Material Name	AL2024-T351
Material Type	Isotropic Elastic-Perfectly Plastic
E	10.5 Msi
ν	0.33
α	12.9 $\mu\epsilon/^0F$
σ_y	47.1 Ksi

Table 3.2: Material data: Graphite-Epoxy [6]

Material Name	AS4/3501-6
Material Type	Orthotropic Elastic
D1111	1.46 Msi
D1122	0 Msi
D2222	9.37 Msi
D1133	0 Msi
D2233	2.97 Msi
D3333	8.67 Msi
D1212	1.11 Msi
D1313	1.11 Msi
D2323	3.34 Msi
α_1	16.0 $\mu\epsilon/^oF$
α_2	-0.51 $\mu\epsilon/^oF$
α_3	3.58 $\mu\epsilon/^oF$

material with elastic-perfectly-plastic deformation behavior. The relevant material constants were specified by the vendor.

The bond material was assumed to be isotropic, elastic-perfectly plastic, with properties as supplied by the vendor.

The properties of the materials used are summarized in Table 3.1, 3.2 and 3.3. The coordinate system in which the graphite-epoxy orthotropic properties are expressed is found in Figure 3-1. The 1-direction is through-thickness, the 2-direction is longitudinal, and the 3-direction is transverse.

Table 3.3: Material data: Film Adhesive [7]

Material Name	FM-123
Material Type	Isotropic Elastic-Perfectly Plastic
E	390 Ksi
ν	0.3
α	40 $\mu\epsilon/^oF$
σ_y	10.3 Ksi
τ_y	5.15 Ksi

3.3.4 Assembly

The three model parts, representing the plug, the tube and the bond, were assembled in CAE such that the upper surfaces (those of circular section) of each aligned at the same station in the 2-direction. Since their diameters were already specified, this was sufficient to constrain fully the parts with respect to each other. The adhesive was 'tied' to the plug on its interior surface and to the tube on its exterior surface. This interaction effectively assumes no adhesive failure.

3.4 Boundary Conditions

The clamp used on the specimens gripped the bottom 1" of the composite tube, which was 4" long. In the ABAQUS model, this boundary condition was enforced by reducing the length of the tube to 3" and requiring displacements and rotations at the unbonded edge of the tube to be identically zero.

In addition, the presence of a closely-fitting bolt through the central hole in the plug necessitated another boundary condition. To keep the plug from overlapping the bolt as it deformed, the interior surface of the hole was denied any displacement in the radial direction.

3.4.1 Loads

ABAQUS allows the application and modification of loads and fields chronologically. Initial conditions are specified in the 'Initial Step', and additional steps are added to introduce or change any environmental condition. Since no stresses were present before joining the specimens, the initial step was specified to be the state of the specimens immediately after curing, while still at the cure temperature.

Thermal Loads

Since the test specimens were bonded before they were tested, thermal stresses were incorporated before the applied mechanical stresses were. To simulate this, a uniform temperature field was created in the initial step. It was applied to the entire assembly. Initially then, the model was stress-free at 240 degrees Farenheit.

The first added step represented the cooldown period of the specimens to room temperature after curing. The isothermal field was brought down to 70F. At this point, the model would determine the thermally-induced stresses caused by the parts undergoing different rates of contraction.

Mechanical Loads

The last step introduced the loads caused by the servohydraulic test machine. The thermal field remained at 70F in this step. The underside of the aluminum plug experienced a uniform displacement in the 2-direction to apply the extraction force.

3.4.2 Meshing

The area of interest in and around the bond is small compared to the overall area of the model. To reduce processing time, large areas of the model were coarsely meshed, while the bond itself had a high resolution. The aluminum plug had the largest area, so large elements were desired away from the bond. However, in order to be compatible with the fine mesh where the plug meets the bond, one side of the aluminum plug also needed to be finely meshed. The plug was seeded with edge nodes using a bias function to set a ratio

of 25:1 between the element sizes at each end. The node spacing in the 2-direction was uniform throughout the model, except in the lower half of the tube, away from the bond, where the spacing was considerably larger. The smallest node spacing in the 1-direction was every 0.003" across the thickness of the bond. After preliminary modeling revealed that the bottom of the bond was the primary area of interest, additional refinement was added in this region. The model was meshed with quadratic, axisymmetric stress elements, referred to in ABAQUS as CAX8 elements.

3.4.3 Analysis and Data extraction

The loads and fields applied to the model were 'ramped' over a step. For the initial 'cooldown' step, the temperature field dropped linearly from 240F to 70F. Multiple frames were taken during each step. At each frame, the field variables were recorded for a fuller understanding of the bond behavior. For the elastic analyses, only one frame was necessary as linear ramps would result in linearly varying results. Analyses in ABAQUS determined component and principal stresses and strains within the bond, as well as nodal displacements. Visualizations of these field variables was completed using ABAQUS/CAE. In cases where averages or extrema were desired, the nodal values of these quantities were exported into Microsoft Excel for processing. Once processed, these results were plotted using Matlab.

3.5 Fracture Analysis

Fracture analyses were carried out using FRANC2D, published by Cornell University. The geometry, loads and boundary conditions used in ABAQUS for the stress analysis were carried over to FRANC2D, but there were some small differences. Firstly, the composite tube was modeled as isotropic rather than orthotropic as it had been in CAE. In addition, meshing was done somewhat differently in the fracture software, to provide sufficient refinement on the interior end of the bond for the fracture analysis. The thermal and mechanical loads were applied in separate load cases. The software calculated the stress intensity factor for each load case separately, as well as for the combined case.

The software was used for the fracture analyses for its ability to incorporate a crack after a model has been generated, and then to remesh adaptively the region around the crack as it propagates.

A crack of length a was incorporated starting at the interior end of the bond, midway between the aluminum and the composite. The software then calculated the stress intensity factor at the crack. By specifying K_c, the critical crack length to propagate the crack at that applied displacement could be found. From this, the failure load and thus the overall strength of the bond could be determined using the load-displacement results from ABAQUS.

Chapter 4

Modeling Results

A depiction of a bonded specimen is included as Figure 4-1, to illustrate reference points mentioned throughout this chapter.

4.1 Elasticity

Figure 4-2 is a plot of applied load versus displacement for a clamped bonded specimen. Both the elastic and plastic responses are plotted.

As can be expected, in the plastic case a smaller load is applied for a given displacement, once a sufficient load has been reached for plasticity to begin. However, comparing the two plots shows that the elastic and plastic curves both reach the average failure load encountered by the strongest specimens, which was approximately 12,500 lbs, at approximately 4.1mil. The elastic and plastic curves do not diverge significantly until loads approach 20,000 lbs. When the extension of the unclamped region of the tube, u_B, is subtracted, this displacement indicates a maximum elastic shear strain in the bond of 6.1%.

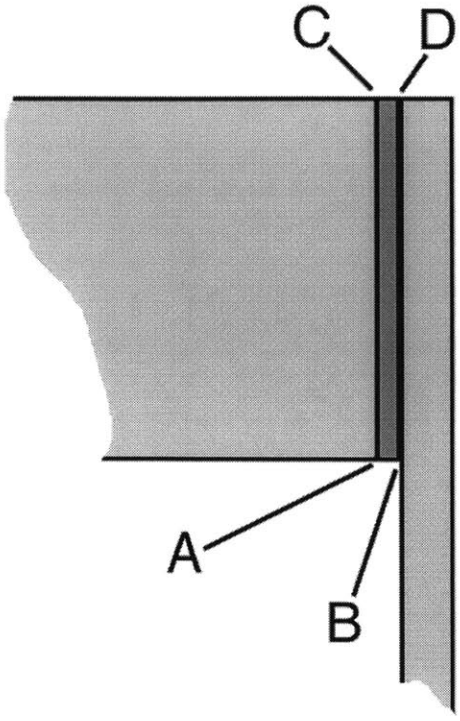

Figure 4-1: Reference locations on bonded specimen

4.2 Strain-Displacement

4.2.1 Cooldown

The total strain experienced in the structure is comprised of elastic, plastic and thermal components. These strains result in displacement of the structural components in three directions. Due to the cylindrical geometry involved, strain in the 'hoop' direction ϵ_{33}, is linked to a displacement in the 1-direction, Δd_1 by Equation 4.1.

$$\Delta d_1 = \epsilon_{33} d_1 \tag{4.1}$$

All of the structural components undergo this diametric reduction after curing at 240F. Since the composite tube and the aluminum plug are far stiffer than the adhesive between them, the difference between their rates of contraction largely determines the strains within the bond. As the structure cools after curing, the spacing between the aluminum and the composite increases. The adhesive expands radially as the plug and tube move apart. Tensile

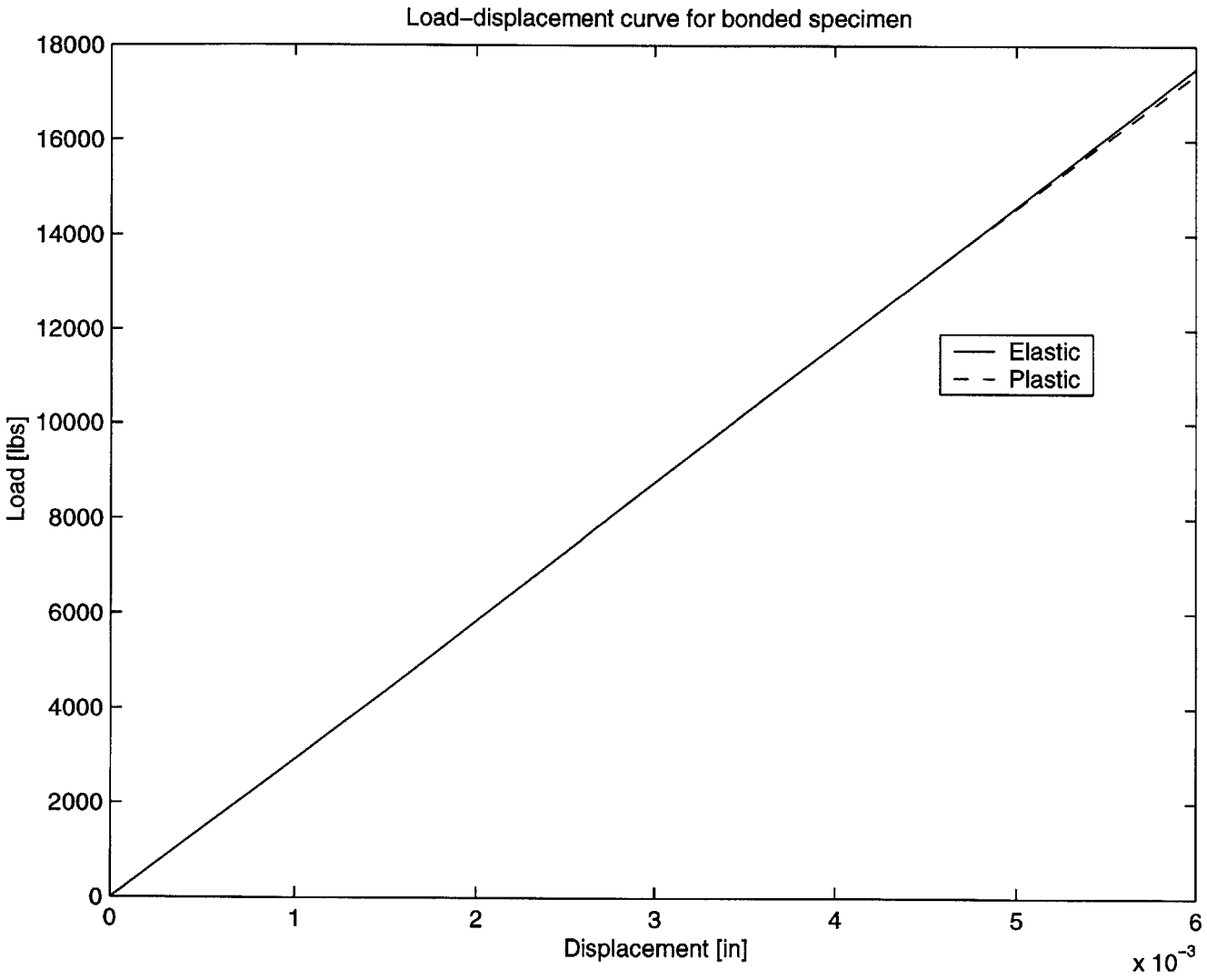

Figure 4-2: Load vs displacement curve for bonded specimen

strain in the adhesive is introduced in the 1-direction through this action.

The adhesive, if unconstrained, would also contract during cooling, but is unable to do so while it remains attached to both adherend surfaces. For equilibrium, this tendency for the bond to contract is overcome by tensile stresses applied to the adhesive by the plug and the tube. After cooling then, the bond is experiencing a positive stress and strain in the 1-direction.

Since the aluminum also contracts more than the composite in the 2-direction, the bond is forced to contract more at its interior surface bonded to the plug, and less at its exterior surface bonded to the tube. As a result, the strain along AC, ϵ_{22}, is smaller than along BD. This gradient of ϵ_{22} in the 1-direction creates a shear strain distribution ϵ_{12}, throughout the bond. Again the bond itself tends to contract in the 2-direction. Since the bond is not constrained in any planes normal to the 2-direction, the bond is able to contract between the two walls, but not at the walls themselves. The bond adopts a concave shape between C and D, and to a lesser extent between A and B.

4.2.2 Loadup

The adhesive material is primarily loaded in shear. Due to the stiffness of the aluminum and the composite, and the uniform displacement of the plug in the 2-direction, the aluminum and composite surfaces stay mostly parallel as they slide against the adhesive. The applied displacement creates shear stresses σ_{12} which transmit the reaction forces holding the tube in place, through the adhesive, to the plug which is being pulled upon.

The creation of shear stresses in the bond compounds the tensile stresses σ_{11} caused by thermal mismatch during the cooldown step. With this additional source of stress, the maximum principal stress in the bond increases. When there are no thermal stresses present, the maximum shear stress in the bond, τ_{max}, equals τ_{12}. The principal stresses are then $[-\tau_{12}, 0, \tau_{12}]$, and are aligned in the coordinate system $[\alpha, \beta, \gamma]$, as illustrated in Figure 4-3, a Mohr's circle showing the stress state in the bond. For comparision, a possible Mohr's circle for the bond with residual tensile stresses through the bond is shown in Figure 4-4.

It is evident from this simplification that the maximum shear stress in the case where

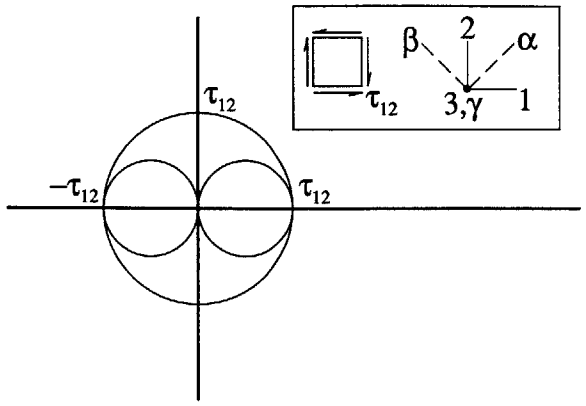

Figure 4-3: Stress Mohr's circle for bond in pure shear

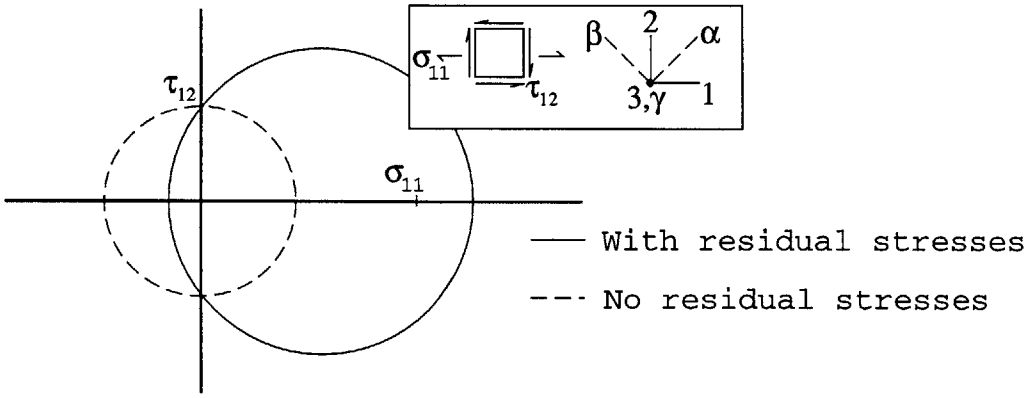

Figure 4-4: Stress Mohr's circle for bond in tension and shear

thermal stresses are non-zero is greater than in the case where there are no thermal stresses present. For these diagrams, the thermal stresses created in the 2-direction were assumed to be zero. However, including normal stresses in the 2-direction would still result in a maximum shear stress greater than or equal to τ_{12}, as long as the 3-direction remains a principal axis.

While it is not generally the case that a Mohr's circle with a greater maximum shear stress has a greater von Mises stress, it is only for specific values of the intermediate principal stress, σ_{II}, that this is not so. Indeed, the intent of the von Mises yield criterion is that yield is governed by the maximum shear stresses in the three planes defined by the three principal directions.

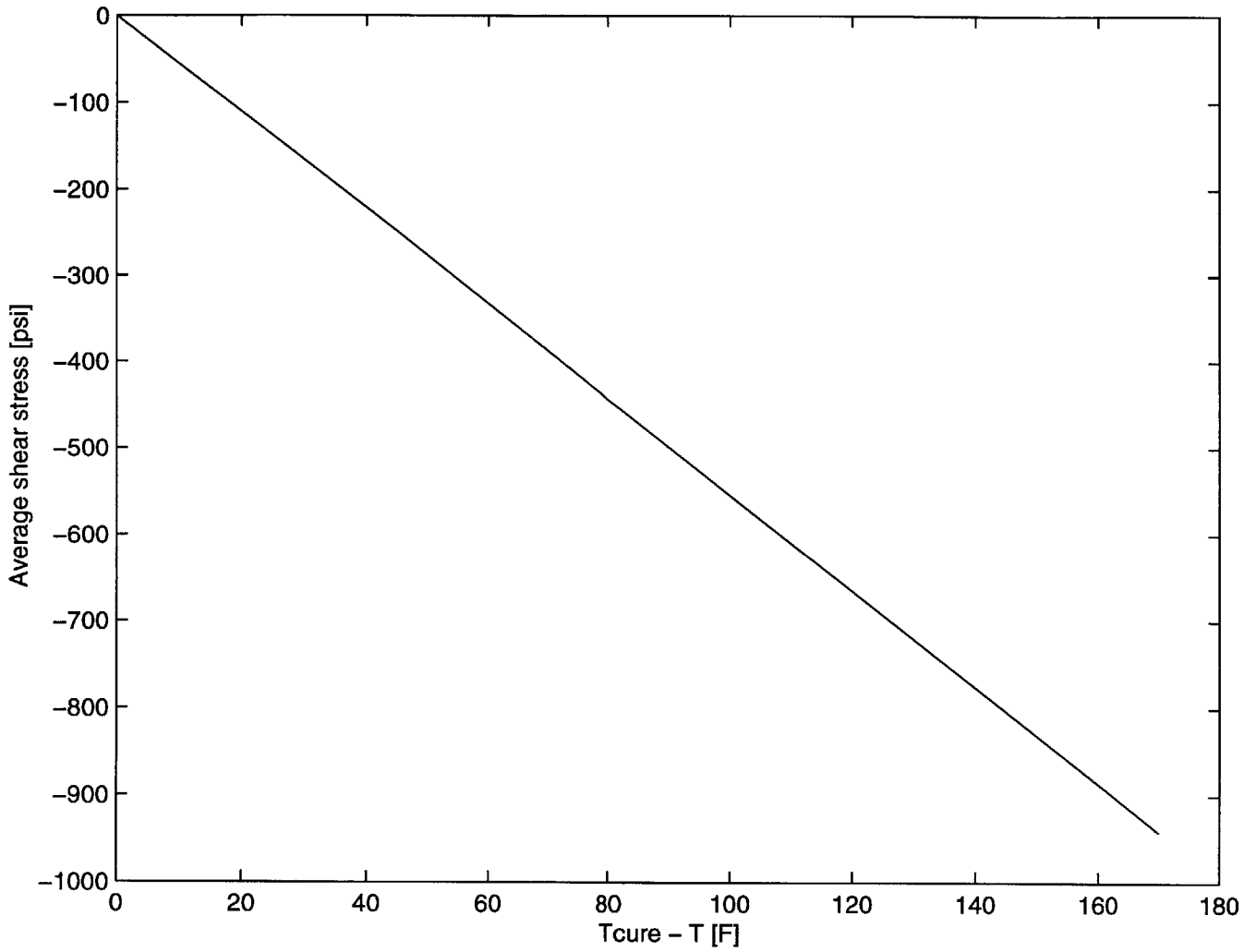

Figure 4-5: Average shear stress in bond during cooldown

4.3 Failure Modes

4.3.1 Maximum/Average Shear Stress

Using an elastic analysis, the average shear stress in the bond (measured at each element centroid), was found to be 4800psi, with a local maximum of 8380psi, when a displacement of 6 mil is applied. Allowing plasticity in the adhesive lowered the average shear stress to 4280psi, with a centroid maximum of 5940psi.

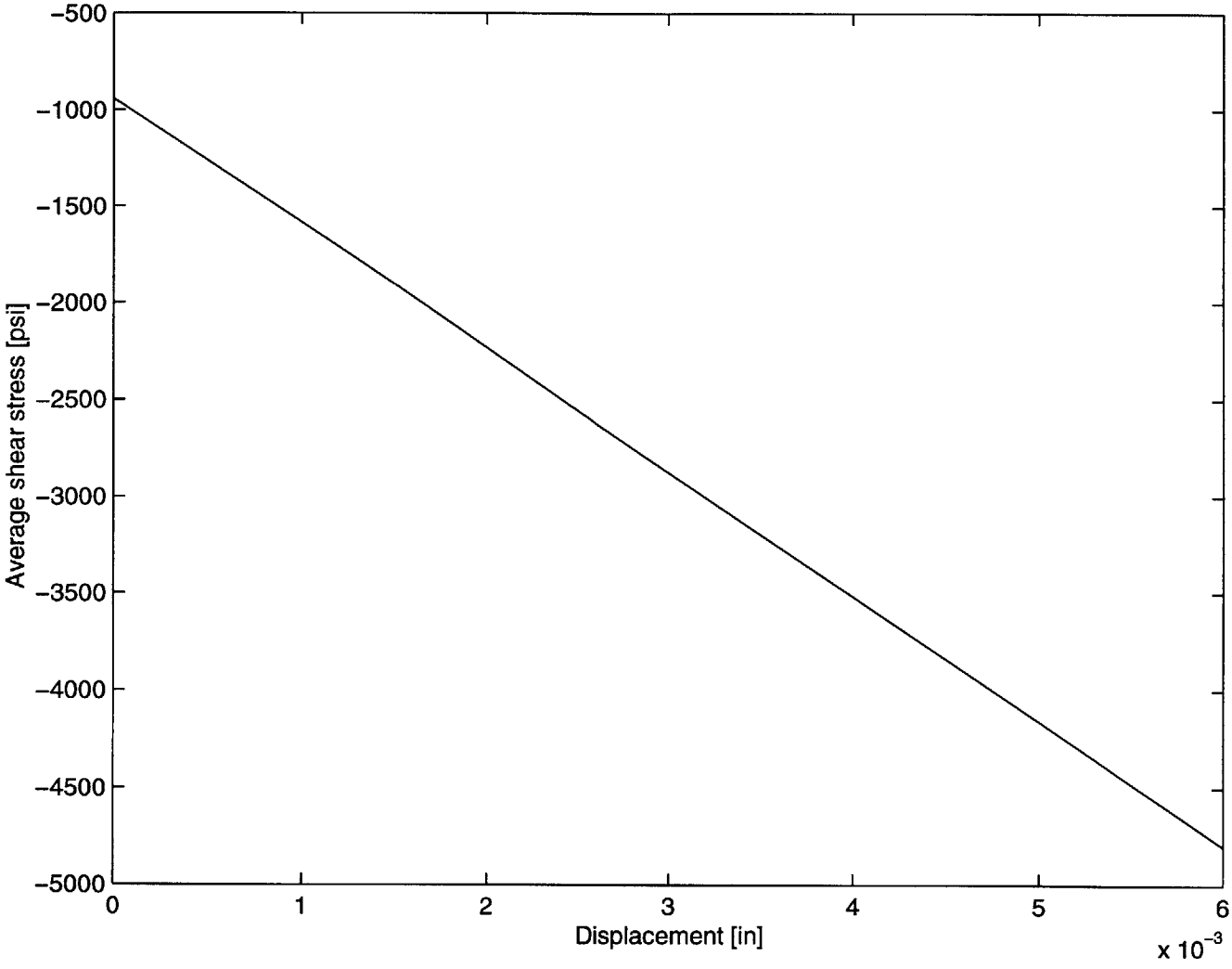

Figure 4-6: Average shear stress in bond during loadup

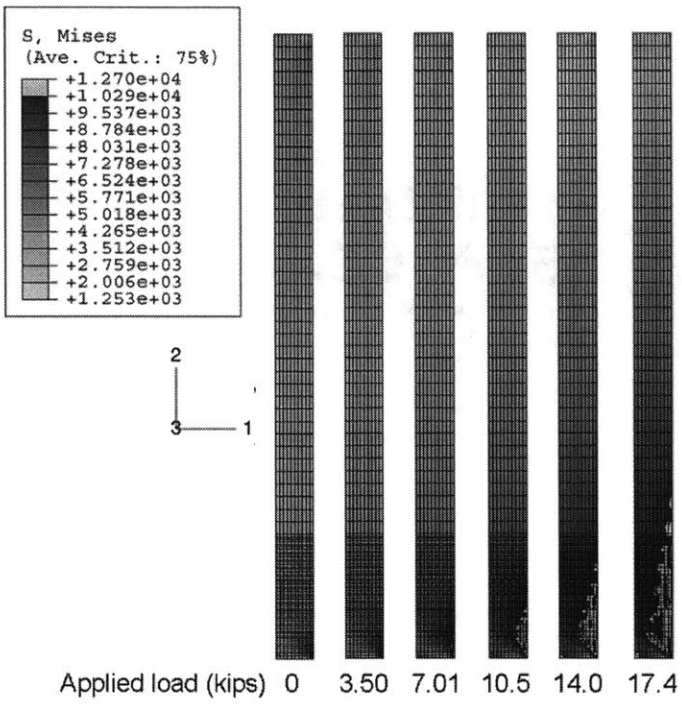

Figure 4-7: Plastic zone growth with applied load

4.3.2 Von Mises Yield Criterion

The von Mises stresses were plotted in the bond for increasing applied displacement. The plastic region of the bond originated near point B, and continued upward and inward with increasing load. The onset of plasticity during the cooldown after curing is minimal. The spread of plasticity during applied displacement is illustrated in Figure 4-7 and the behavior local to point B in Figure 4-8. The von Mises stresses in the bond after cooldown are shown in these figures as the zero load image. The percentage of the bond that has reached the yield stress of the adhesive is plotted against applied load in 4-9.

After cooling to room temperature following the bond cure, specimens bonded with FM-123 film adhesive are estimated to experience a plastic zone in 0.2% of the bond area, around point B. When subsequently loaded by a uniform displacement to approximately 14,000 lbs, the plastic region spreads to cover 14.3% of the bond area. Initially this spread proceeds upward in the direction BD, then through the thickness of the bond towards point C, but the plastic zone remains local around B.

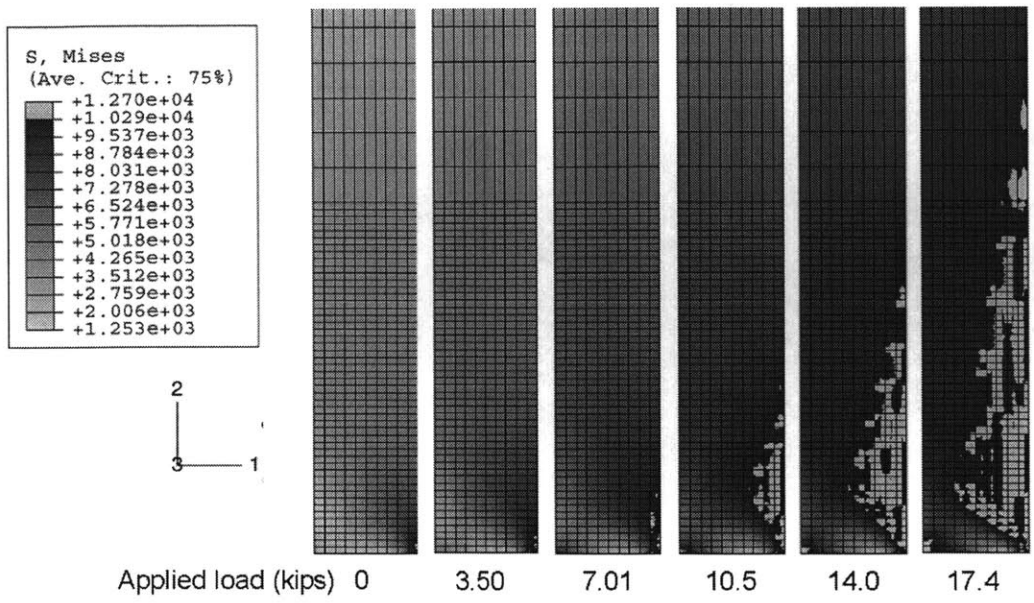

Figure 4-8: Plastic zone growth locally around point B

4.3.3 Strain Invariant Failure Theory

The first strain invariant was extracted from ABAQUS for the bond region of the model. The average values are plotted against load in Figure 4-10. The values at zero applied load correspond to the strain caused by post-cure cooling. Since the cooldown process is elastic, these values vary linearly from zero at the cure temperature. The thermal strains generated during cooldown remain constant while displacement is applied. The elastic, plastic and thermal strains are summed and plotted as Total strain. Elastic strain in ABAQUS is all mechanically-induced strain up to the strain at which the elements undergo plastic deformation. In elements that have undergone plastic deformation, the elastic strain is at a maximum, and the plastic strain is positive. Thermal strain is strain caused by a temperature field which changes spatially or temporally. Boundary conditions or thermally-mismatched materials may induce elastic strains due to a change in temperature when there are no externally applied loads present. The sum of these three components (when creep strain is zero), is referred to in ABAQUS as total strain.

While the elastic strain invariant is positive, inclusion of the thermal strain shifts the curve downward, so the invariant remains negative under applied displacement, with only

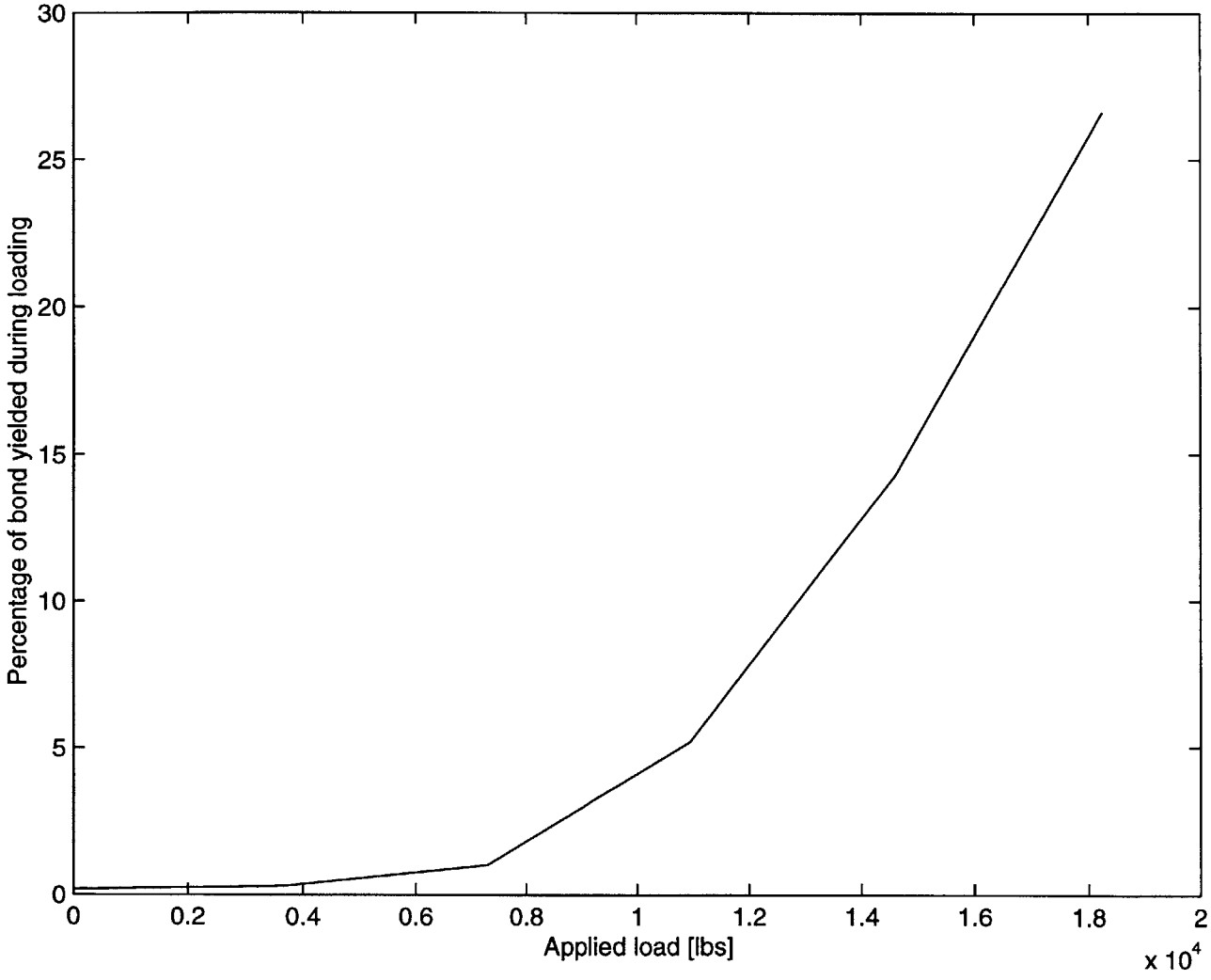

Figure 4-9: Bond plasticity percentage during loading

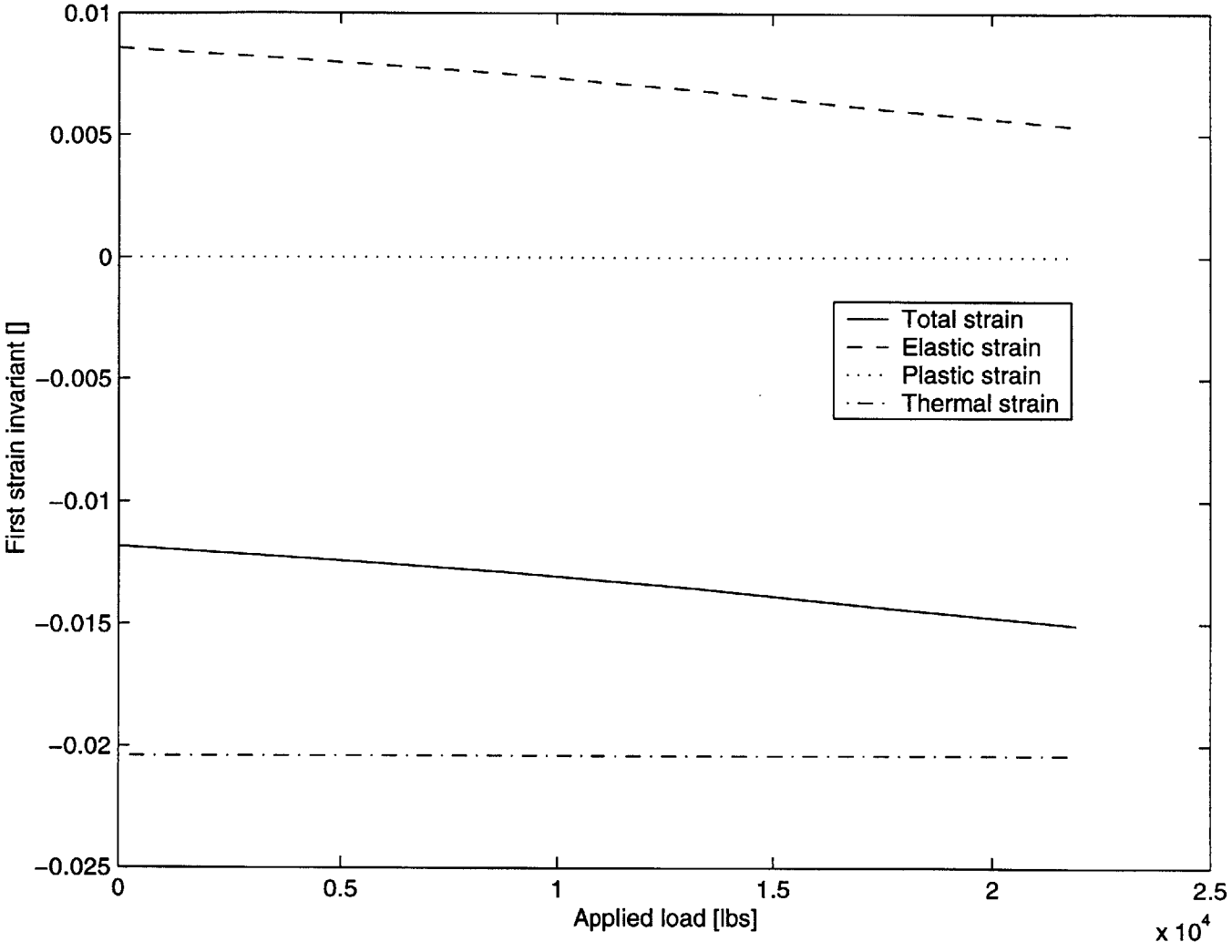

Figure 4-10: Average first strain invariant during loading step

small variation.

4.3.4 Fracture

A plot of K_{II} against initial crack length is included as Figure 4-11, for a crack extending into the bond from the midpoint of AB. The mode II stress intensity factor, K_{II}, is calculated using the FRANC software by both the J-integral [27] and Displacement Correlation methods [28]. The structure experienced the same loading as was applied for the stress analysis in ABAQUS. The structure was cooled down from 240F to 70F, and subsequently a uniform displacement was applied to the bottom edge of the aluminum plug. The curve reaches a constant when the initial crack length exceeds approximately 0.03". Figure 4-12 shows the linear relationship between K_{II} and applied displacement, u, in the linear elastic regime of the model.

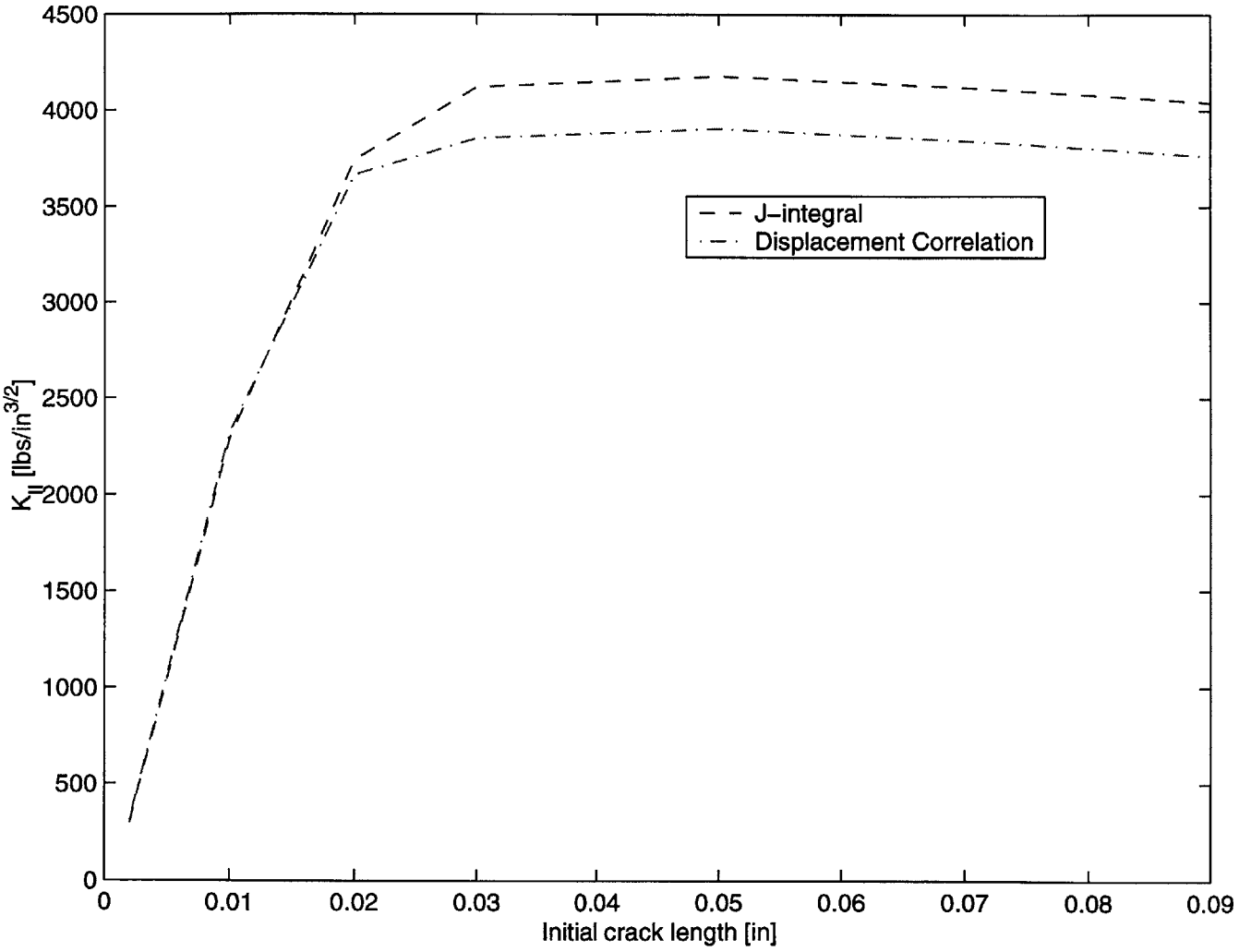

Figure 4-11: Mode II stress intensity factor (K_{II}) under thermomechanical loading

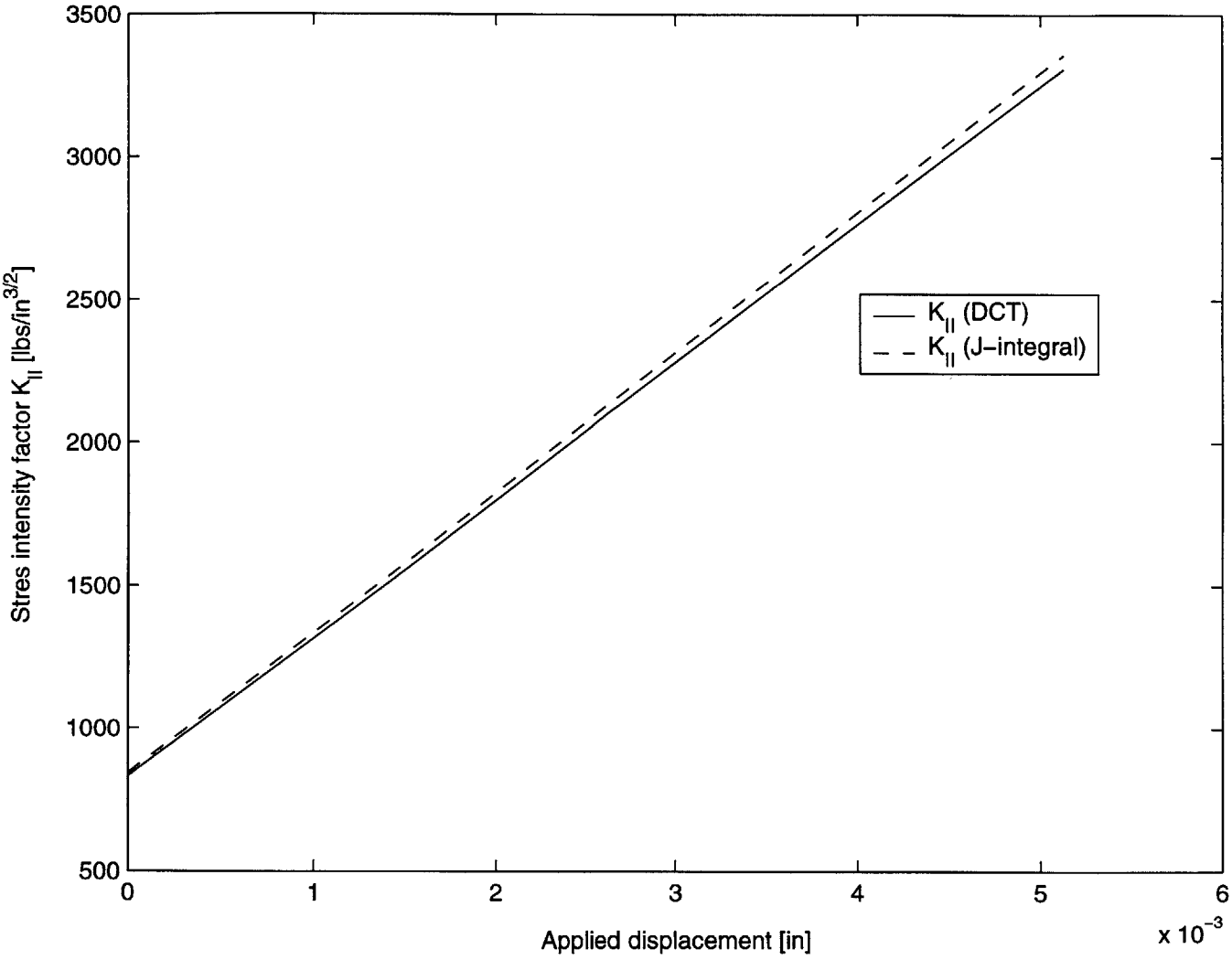

Figure 4-12: Mode II stress intensity factor (K_{II}) against applied displacement

Chapter 5

Experimental Procedure

5.1 Introduction

This chapter describes the experimental work that took place as part of this project. Manufacturing and joining methods are presented, as are preparation details for the specimen adherends. Extensive remarks on the experimental set-up are given, followed by testing and data collecting procedures. The chapter concludes with a matrix of tests completed, decribing the combination of surface preparation and joining method used in each.

5.2 Specimen Manufacture

In this section the methods employed are presented to produce the two components of the joined test specimens. The graphite-epoxy tubular laminates were fabricated using the facilities of TELAC, and were machined by Mr. Peter Morley of the MIT Central Machine Shop. The aluminum plugs were cut in the Gelb Laboratory in the Department of Aeronautics and Astronautics.

5.2.1 Composite Tubes

Graphite-epoxy tubes were made from AS4/3501-6 pre-impregnated tape ("pre-preg") using the TELAC lab facilities. The stacking sequence of the pre-preg plies was $[0\pm45]_{3s}$, with the

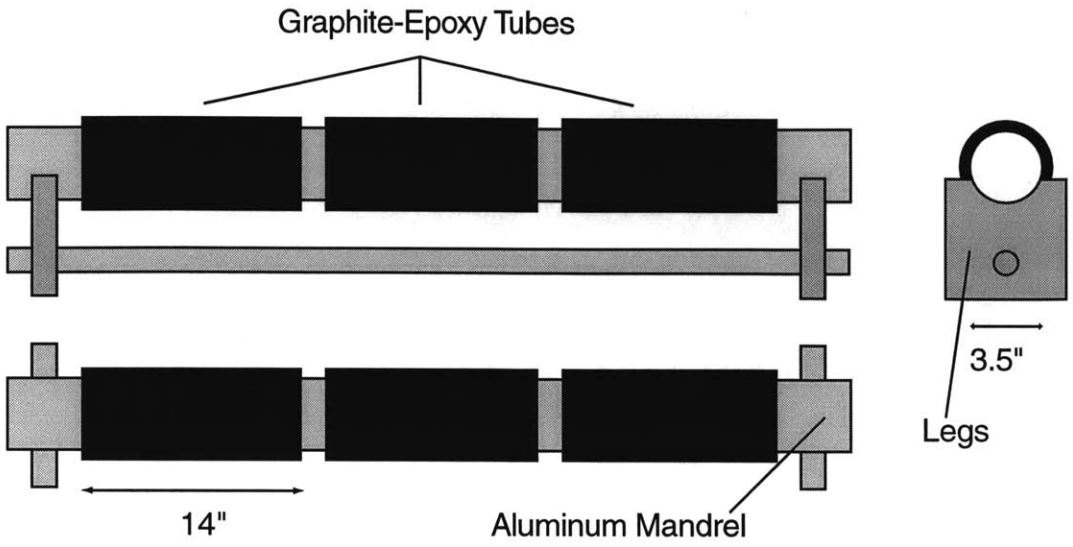

Figure 5-1: Three tubes layed up on aluminum mandrel

0 degree datum aligned with the longitudinal axis of the tube.

Lay-up

An aluminum mandrel measuring 5' x 3.5" diameter was used for laying up the laminates. Firstly, the mandrel was treated with Mold-Wiz and wrapped in non-porous teflon which was secured in place using 3M spray adhesive. The mandrel was to accommodate 3 laminates in a line, as shown in Figure 5-1, and so flash tape was wrapped at 3 locations on the mandrel as references for beginning the layup.

A spool of pre-preg was removed from cold storage and allowed to warm for one hour before unwrapping, to reduce condensation forming on the cold material. Plies were cut using 0 and 45 degree templates to make sheets measuring 12" by 14". Since the circumference of the laminate increased with each additional ply, the sheets were each trimmed down from 12" to the specific dimension required to abut itself exactly when wrapped. Care was taken to ensure no air was enclosed when wrapping plies. Following layup of all three laminates, the mandrel was transported to the autoclave room to be bagged for an autoclave cure.

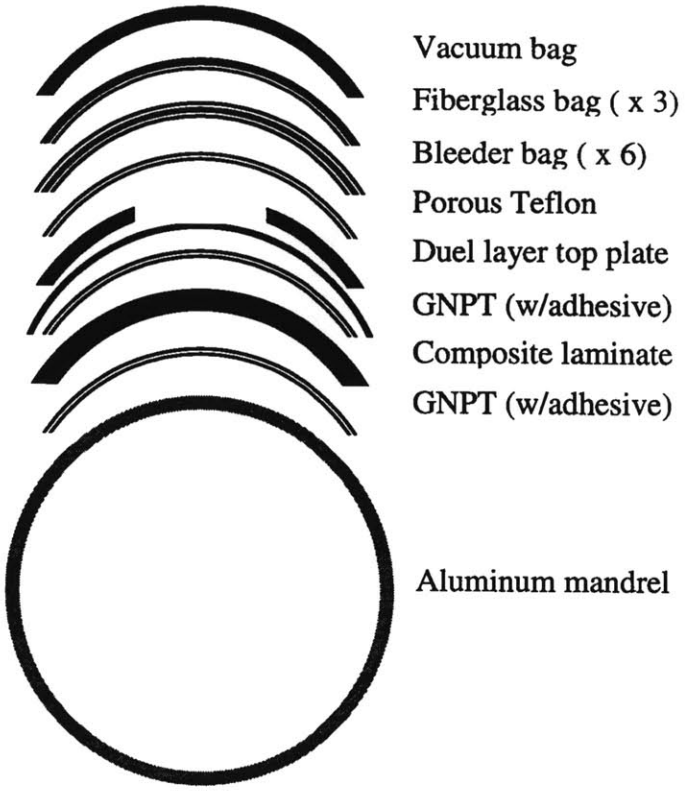

Figure 5-2: Schematic of bagging material placement

Curing

To prepare the laminae for curing, the tubes had to be wrapped in a variety of materials. The wrapping sequence was succesfully determined by Kessler [8]. The first layer wrapped around the plies was GNPT, so that the cured tubes would not stick to the other curing materials. Next a dual layer metal top plate was tightly wrapped and generously taped to give the tubes a consistent thickness and surface finish. Porous teflon, bleeder paper and fiberglass were then wrapped to channel away and absorb excess epoxy, and to maintain vacuum. Finally the vacuum bag was wrapped and secured with vacuum tape at both ends, and along the length, of the mandrel. The bagging profile is reproduced from Kessler in Figure 5-2.

The autoclave cure followed a standard TELAC cure cycle. Firstly, a vacuum was pulled on the mandrel, removing the air from the laminae. Next, the internal pressure in the autoclave was increased to 85 psi, with a corresponding increase in internal temperature. At

85 psi, the autoclave heater was activated, and the thermostat set to 240 degrees Farenheit. The cycle was held at this temperature for one hour, to allow the epoxy to gel. Next the thermostat was turned up to 350 degrees, at which the temperature was held for 2 hours. Next, the autoclave was cooled at 5 degrees per minute down to 150 degrees, and then left overnight.

Finishing

The procedure for removing the tubes from the mandrel is time-consuming. Despite thermal contraction loosening the mandrel from inside the cured laminates, the static forces acting on the large contact areas of the tubes made removal a very gradual process. The mandrel sits on two 'legs' which are shaped to hold the mandrel on semicircular supports. The legs are separated and held upright by a long threaded rod with two bolts surrounding each leg. By progressively loosening and tightening pairs of bolts, the legs were used to slide the laminates along the mandrel and off one end.

Once removed from the mandrel, the three 14" tubes were post-cured for 8 hours at 350 degrees in the TELAC post cure oven to achieve a greater than 99% cure.

Each of the 14" tubes was cut into three shorter, 4" long tubes using a continuous carbide grit bandsaw blade. This work was contracted to the MIT Central Machine Shop.

5.2.2 Aluminum Plugs

Disk-like plugs were manufactured from Aluminum 2024-T351. Outer diameters ranged from 3.490" to 3.510" to work with different joining systems, and each plug was 1/2" thick. Each plug had a 1"-diameter hole at the center to accommodate the bolt connecting the specimen to the loading grips. The specimens were manufactured in batches using an Omax water jet cutter in the Gelb Machine Shop at MIT from a single plate of 1/2" aluminum.

5.3 Specimen Preparation

Previous work by Barbara Huppe [2] highlighted the importance of proper adherend surface preparation for adhesive bonding, and the strong dependence of bond strength upon it. Adherends were prepared in a number of ways. In some cases, these preparations were intended to maximize the bond strength and minimize variation between similar specimens. In other cases, the preparations were intended to simplify manufacturing procedures or provide control cases for comparison.

5.3.1 Composite Tubes

Tubes were prepared using one of two procedures, depending upon the joint for which they were intended. Nine tubes were sanded using 600-grit sandpaper, using an axial and circumferential motion. Tubes were only sanded in the region to be bonded. Sanding continued until the carbon powder removed had gone from dark green to black. Immediately after sanding, the abraded surface was wiped with damp Kim-wipes and then dried with the same. Bonding of the tubes immediately followed sanding.

Three specimens were wiped with damp Kim-wipes, and dried. The remaining three specimens were neither cleaned nor sanded, later to be fastened to aluminum plugs using standard machine screws.

5.3.2 Aluminum Plugs

The plugs cut by water jet were not, in general, further machined. In some cases, a small seam protruding across the thickness of the plug was ground down using a rotary sander until flush with the remainder of the plug surface. The affected region was typically a band no wider than 0.1" running across the thickness of each plug.

A batch of aluminum plugs of various diameters were etched using BR-127 chemical etchant and subsequently primed to promote maximum adhesion between the aluminum surface and the adhesive systems used.

Plugs that were not etched and primed were sanded with 600-grit sandpaper prior to

bonding, to remove the aluminum oxide layer on the plug surfaces.

5.4 Joining

Plugs were joined to tubes using one of three different procedures. There was a method for joining using film adhesive, a method for joining with epoxy, and a third for fastening using screws.

5.4.1 Film Adhesive

The film adhesive used was Cytec FM-123. The adhesive is paper-backed, and at cool temperatures can be cut to a planar shape with scissors and applied to a bonding surface.

The bonding surface of one aluminum plug measured 3.5" by 0.5". Film adhesive was cut to 3.5" by approximately 1.5". The adhesive was wrapped circumferentially, so that the ends of the film adhesive would abut each other, and so that there were equal widths of excess film adhesive extending upward and downward from the bonding surface. These excesses were then folded down onto the top and bottom surfaces of the plugs. The purpose of this excess film was to anchor the adhesive so that it would not 'bunch up' as the plug was inserted into a tightly fitting plug. Allowing adequate spacing for the film adhesive is also critical for achieving successful plug insertion.

After assembling the bond, the joint was cured in the TELAC post cure oven at 240 degrees Farenheit for two hours.

5.4.2 Liquid Epoxy System

West System Epoxy 105 resin and 205 hardener were mixed in the instructed ratio of 5:1 immediately prior to bonding. The outer curved surface of each prepared plug was brushed liberally with the epoxy mixture and placed on a flat cure plate covered by non-porous teflon ("NPT"). Then, the interior surface of a composite tube was brushed with the epoxy mixture, and lowered around the plug. Excess epoxy simply flowed out from underneath

onto the NPT. This could be easily chipped off the exterior plug surface after curing. The assembly was left to cure for a minimum of 24 hours at room temperature.

5.4.3 Mechanically Fastened

Mechanically fastened specimens incorporated a set of four 1/4"-20 machine screws, which were inserted at 90 degree increments. An unprepared plug was inserted into a composite tube until one surface of the plug was flush with the end of the tube. This plug was secured in place and a set of conventional, high-speed steel drills was used to cut holes through the tube and into the midplane of the plug. The two materials were drilled in unison to ensure the holes would line up properly. The holes were opened up to 0.201", at which point the plug was removed and tapped for 1/4"-20 screws. The holes through the tube were then further opened for a normal fit for a 1/4" screw. The two parts were reassembled and the fasteners screwed in place.

5.5 Testing Apparatus

The jointed test specimens were to be installed in a servohydraulic load frame so that the metal plug could be extracted from the composite tube. Since failure of the adhesive joint at the top of the tube was desired during each tensile test, the bottom end of the tube had to be secured against slippage or damage up to the failure load of the adhesive joint.

To accomplish this, a clamp was devised and implemented as an interface between the bottom end of the composite tube, and the lower set of hydraulic grips on the load frame. A diagram of the clamp is included as Figure 5-3.

The clamp was made up of the following parts.

- A support *seat*,
- An internal *plug*,
- An annular *wedge*, and
- A clamping *ring*.

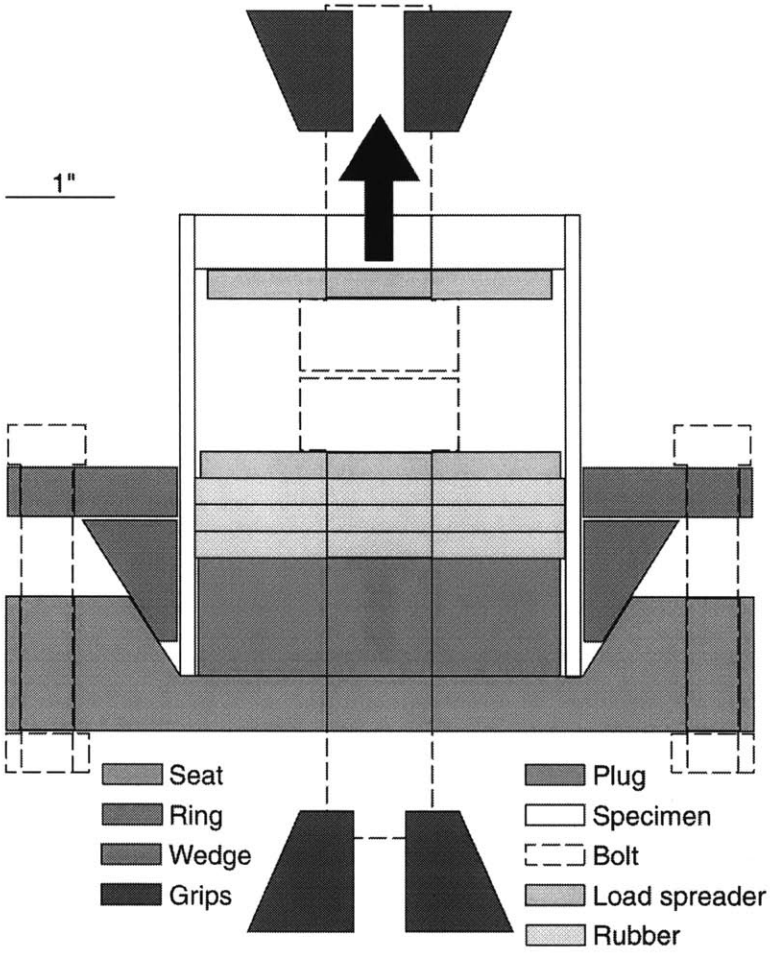

Figure 5-3: Clamp for securing test specimen

Both the ring and the seat featured an eight-bolt circle.

The clamping device works as follows.

Firstly, the plug was inserted into the bottom end of a composite tube specimen. The two were then placed into the seat, and centered automatically by a protrusion of the plug fitting into a complementary cut into the seat.

Secondly, the wedge part, which is C-shaped, was lowered around the tube into the seat, which features a taper to match that of the wedge. (For tubes with protruding boltheads, the wedge was slid up from the bottom end before seating the tube and plug.) Next, the ring was lowered on top of the wedge and rotated to match up bolt holes with the seat.

Finally, bolts were inserted up through the seat, also passing through the ring, and were secured with lock washers and nuts. Progressive tightening of opposing pairs of bolts drove the wedge downward and inward (because of the taper), clamping the tube between the wedge and the plug.

While this procedure results in a properly clamped specimen, it does not fully describe the test assembly. In order to conduct a pull-out test in the load frame, the assembly had to be clamped, top and bottom, in the hydraulic grips of the MTS machine. To address this, both the plug and seat parts of the clamp featured a 1"-diameter hole through their centers, as did each of the joined specimens.

A load spreading device sharing the planar section of the aluminum adherends, but fashioned out of 1/4" thick stainless steel, was slid onto a 1"-diameter bolt and that assembly was inserted upward through the hole in the test specimen. Another similar bolt was inserted downward through the steel plug and seat of the clamp. After considerable revisions to the testing procedure, this setup came to include 3 plies of 80A durometer, 1/4"-thick rubber, located on top of the steel plug and beneath a steel shim identical to the load spreader used at the top end.

The resulting assembly featured threaded, 1"-diameter bolts, extending both upward through the center of the test specimen and downward through the clamping device.

5.5.1 Load frame installation

For proper alignment, the test assembly was first gripped in the upper grips of the MTS load frame. Since the total weight of the test assembly approached 25 pounds, the test assembly was supported on two sections of 2"x4" pine while the upper grips were closed around the top bolt. The lower head of the load frame was then lowered and the wooden supports removed. Finally the lower head was raised, causing the bottom bolt to insert itself between the bottom set of grips. These grips were then clamped shut, resulting in a fully installed test assembly, as previously shown in Figure 5-3.

5.6 Testing Procedures

5.6.1 Calibration

The position measurement of the load frame had been previously calibrated on-site by an Instron technician. The load measurement for the MTS 100,000 pound load cell was recalibrated at the start of testing each day using the automatic calibration feature of the system. Additional recalibrations took place throughout the day, whenever excessive drift from zero load was observed. Typically, these additional calibrations were unnecessary. The MTS load cell tended to drift very slowly, often only a few tens of pounds over a weekend.

5.6.2 Loading

The specimens were loaded axially in displacement control in an MTS servohydraulic load frame. Tests were conducted by setting a head velocity of +0.05" per minute. The lower head would move downward at this rate while the upper head remained stationary, resulting in an upward pressure on the aluminum plug as the assembly descended.

5.6.3 Data Collection

The Instron instrument panel controlling the MTS machine was set up to output load measured by the MTS load cell and position of the lower head continuously. This two-channel

data stream was sampled at 1-4Hz using a National Instruments NiDAQ board, and recorded using LabView 5.0 on a Macintosh computer. The data was appended to a time base generated independently by the LabView program.

In addition to load and position data, details of each test were recorded qualitatively before, during and following the loading phase.

Before the specimen was installed into the test assembly, any visually-detectable defects were recorded and marked on the specimen, and a reference marked to show how the plug and tube lined up before they were separated.

During the test, events such as audible cracking or visible deformation were logged. Specimen slippage was also noted so that position data for such tests could be treated appropriately. Any breakage that was not axisymmetric was logged, else the test was considered "straight pull-out".

Following each test, the test assembly was removed from the load frame, and both the plug and tube were inspected, particularly the regions where defects had been previously observed. Details of damage type and extent were noted. Digital frame captures were taken of the details of the failed joint using a Zeiss stereoscope and a Hewlett-Packard digital camera.

5.7 Test Matrix

Different joining techniques and surface preparations were combined to fill out the testing program for this project. Six tests were completed using film adhesive. Of these, three of them bonded sanded composites to primed plugs. The remaining three were cleaned composites bonded to sanded plugs.

A further six tests used a liquid epoxy adhesive system to bond the adherends. In each case the tubes were sanded and the plugs primed, but the plugs were three each of two diameters, differing by 0.030".

The last set of specimens were mechanically fastened using a set of machine screws, and so did not receive any surface preparation beyond cleaning both surfaces.

These tests are summarized in Table 5.1.

Table 5.1: Test matrix

	Surface Preparation	
Joining Method	Primed & Sanded	Cleaned
FM-123	3	3
105/206, loose	3	0
tight	3	0
Fastened	0	3

Chapter 6

Experimental Results

6.1 Bond Strength

The strongest bond was obtained using sanded composites bonded to primed aluminum plugs. The epoxy system used for the strongest specimens was West Systems 105/205. Using smaller plugs for a thicker bond yielded a slight increase in mean failure load, but the increase was not statistically significant.

The sanded/primed specimens bonded using film adhesive were the next strongest set of specimens. The mean failure load of these specimens was approximately 1000 lbs less than the mean failure load of the entire sanded/primed 105/205 specimen set.

The specimens comprised of sanded aluminum and cleaned composite had a bond strength significantly lower than any of the sanded/primed specimens. In addition, these specimens had the greatest spread between their failure loads. The standard deviation of their failure loads was 2071lbs, which is two to five times greater than that of the other adhesively bonded specimens.

The maximum load experienced by the mechanically fastened specimens was far lower than that of the adhesively bonded specimens. With four screws used, the fastened specimens were about 20% as strong as the sanded/primed specimens.

To determine the nominal strength of the joint, the failure load is divided by a characteristic area. For the adhesive joints, this is the area of the curved outer surface of the plug,

Table 6.1: Failure load

	Surface Preparation		*Failure Load*			
Joint	Composite	Aluminum	1	2	3	
FM-123	Cleaned	Sanded	5124	7032	7834	lbs
FM-123	Sanded	Primed	11592	12206	12966	lbs
105/205	Sanded	Primed	12740	12941	13276	lbs
105/205 (tight)	Sanded	Primed	12989	13281	13708	lbs
1/4"-20 screws	Cleaned	Cleaned	2104	2767	2991	lbs

Table 6.2: Statistical information

	Surface Preparation		*Failure Load*			
Joint	Composite	Aluminum	Mean	Standard Deviation		C.O.V.
FM-123	Cleaned	Sanded	6664	1392	lbs	0.208
FM-123	Sanded	Primed	12255	688	lbs	0.056
105/205	Sanded	Primed	12986	271	lbs	0.021
105/205 (tight)	Sanded	Primed	13326	362	lbs	0.027
1/4"-20 screws	Cleaned	Cleaned	2621	461	lbs	0.17

or 5.5 in^2. For the mechanically fastened specimens failing by shear out, the relevant area of is that which is torn through by extraction of the screws, which is 0.2 in^2. Naturally, the strength of the composite averages far higher than that of the adhesive. It is reasonable then that increasing the number of screws could increase the area to be torn out, and correspondingly increase the failure load, until failure by shear out is preempted by net tension failure.

The maximum load experienced by each specimen are listed in Table 6.1, and represented graphically in Figure 6-1. Mean failure load, standard deviation and coefficient of variation (C.O.V.) are included in Table 6.2.

6.2 Failure

Every adhesive specimen failed instantaneously with a large deformation and a sharp drop in applied load. In most cases, the plug extracted fully from the composite tube. In other

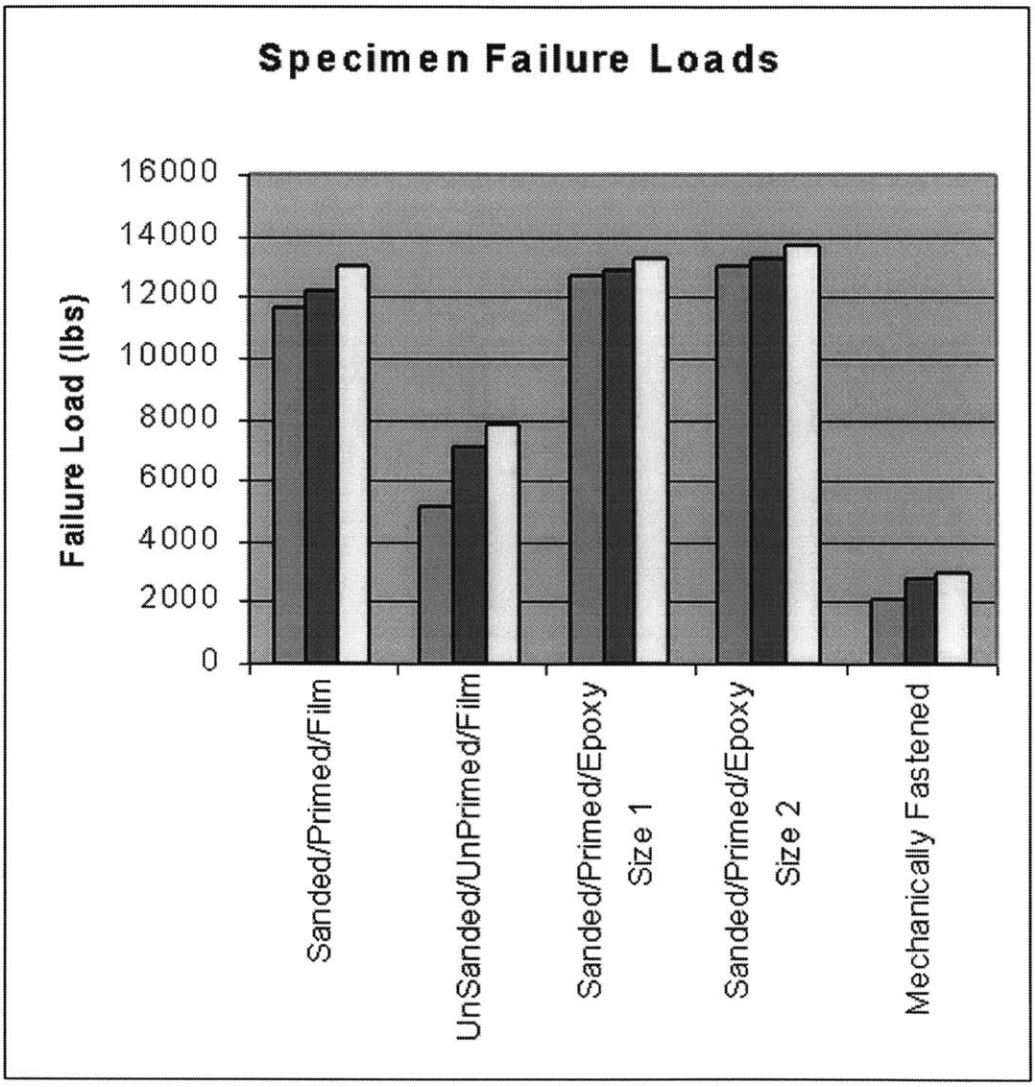

Figure 6-1: Variation in specimen failure load with surface preparation

cases, the plug failed on one side, and steadily pulled out at a load less than 5% of the maximum load experienced.

In all adhesive cases, there was no visible displacement of the plug before major failure. High-pitched cracking was heard during the last 5 to 10 seconds before failure, while within approximately 1500lbs of maximum load. The applied load did continue to increase, however, right up until catastrophic damage occurred. This behavior is indicative of failure by fast fracture.

When fastened specimens were tested, they failed very differently from the adhesive specimens. The screws remained firmly inserted in the tapped aluminum plugs during the entire test. Like the adhesively-bonded specimens, the fastened joints experienced a sharp dropoff in load and significant damage after reaching some maximum load. This dropoff was accompanied by two of the four screws tearing through the composite tube, leaving two still in place. After the slack was taken up, the remaining screws were again loaded until one of them also sheared out, typically peaking at about 50% of the maximum load endured. Again the slack was taken up, and the remaining screw pulled out at a further reduced load.

6.3 Observations of failed components

6.3.1 Composite tubes

Cleaned

Tubes which were only cleaned before adhesive bonding had minimal visible damage after joint failure. There was greater than 90% adhesive failure between the film adhesive and the tube. It was difficult to distinguish between the previously-bonded area of the tube and that which was left unbonded. The only visible evidence the tube had even been used were small patches of film adhesive which had failed cohesively, remaining attached to the tubes. The undamaged appearance of the tube after joint failure is indicative of the highly superficial adherence achieved between the film and the composite.

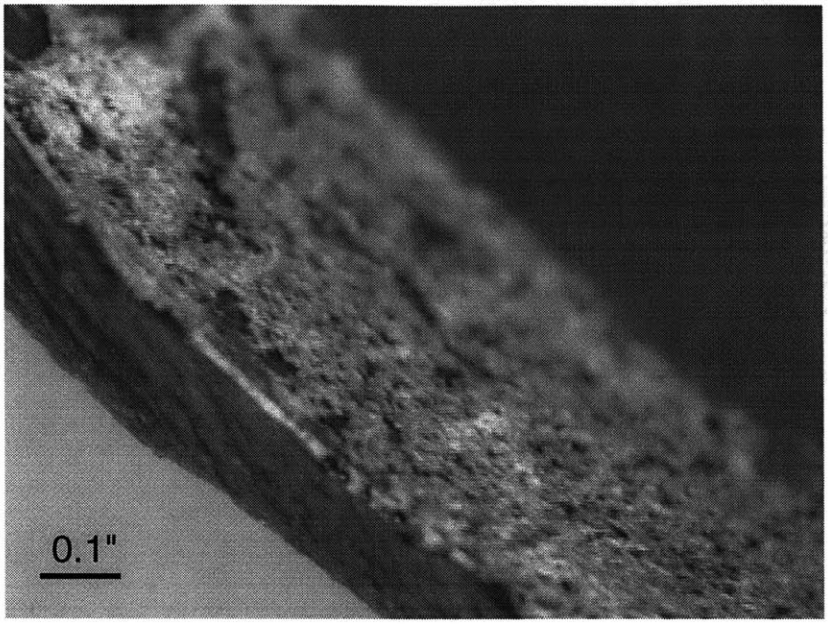

Figure 6-2: Interior tube surface with broken film adhesive remains

Sanded

Sanding the composite tubes was an effective surface preparation. Adhesive failure between the film and the tube was very much reduced when sanding rather than simply cleaning. When film adhesive was used, the tubes after pull-out displayed a mixture of cohesive failures, both in the adhesive and in the tube. Failed film adhesive remaining on a tube specimen can be seen in Figure 6-2. Cohesive failure of the tube varied between loss of surface fibers and breakage of up to two plies of the laminate. The former effect was typical when epoxy was used as the adhesive. The latter occurred often when using film adhesive. Breakage was categorized by ply 'splintering' or plug attachment. These effects are shown in Figure 6-3 and 6-4, respectively.

Drilled

The drilled composite tubes were all damaged consistent with bolt shear out failure, as shown in Figure 6-5. Photographs of a failed composite tube are included as Figures 6-6 and 6-7.

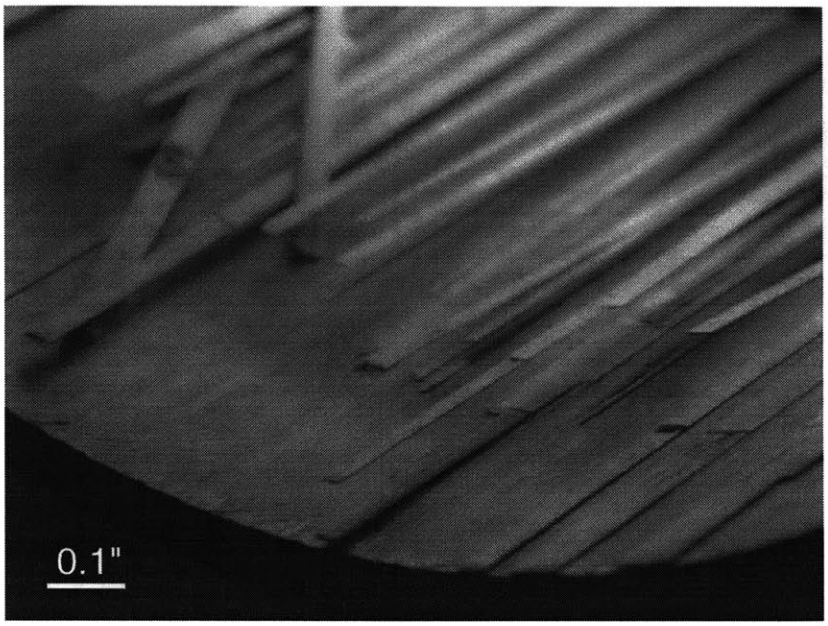

Figure 6-3: Interior tube surface showing splintering damage

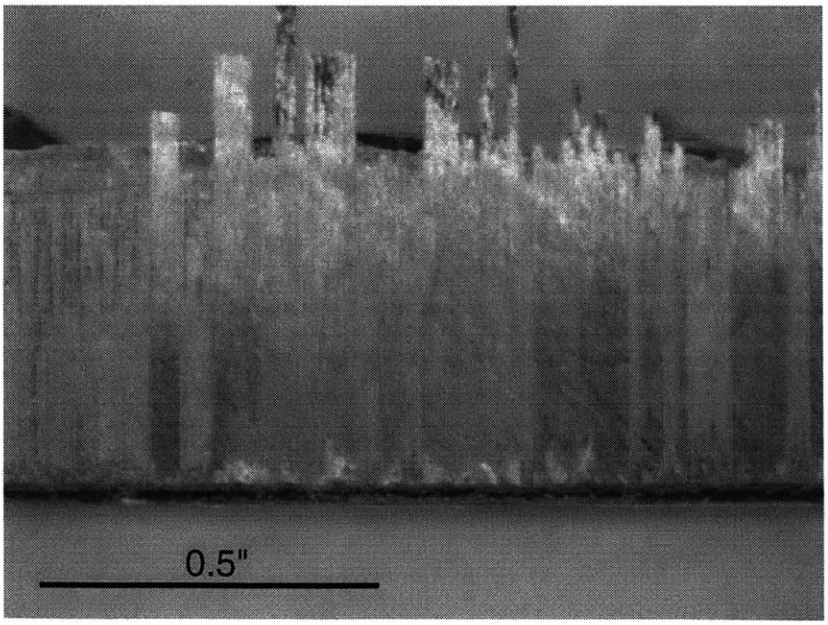

Figure 6-4: Plug exterior surface showing adhered plies

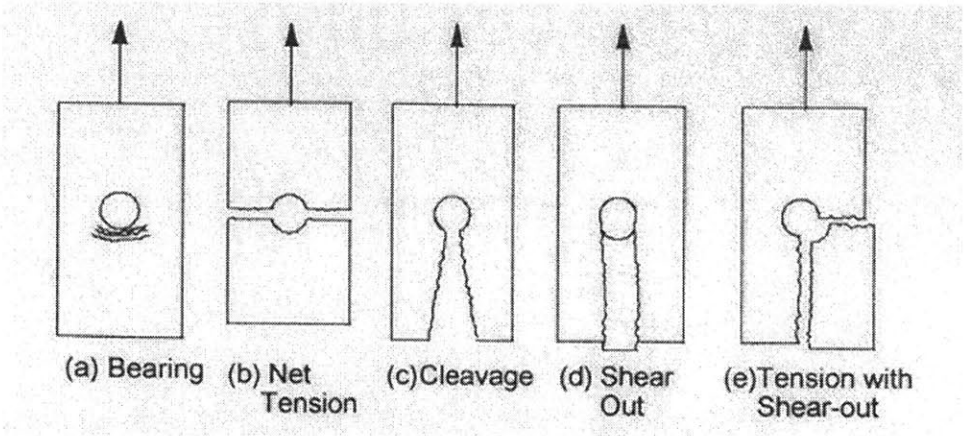

Figure 6-5: Typical modes of failure of FRP bolted connections [4]

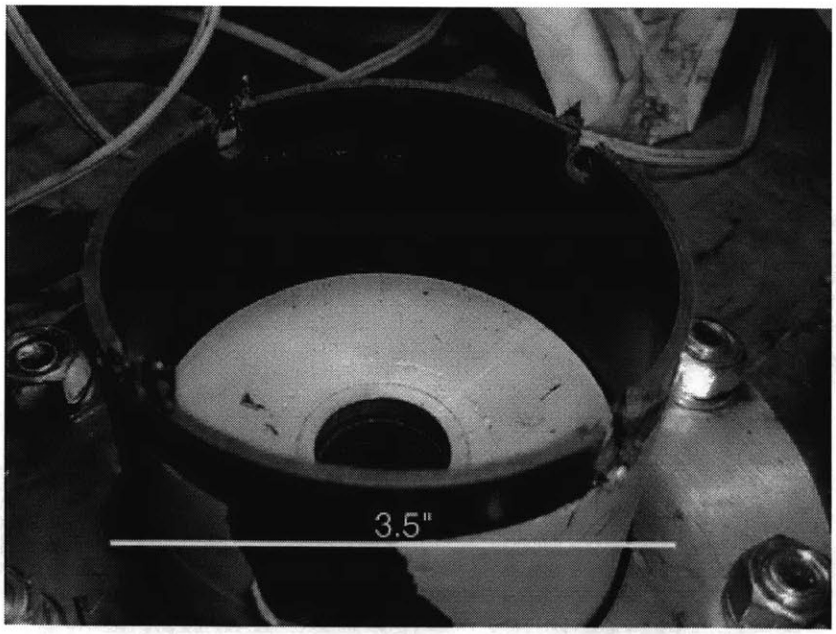

Figure 6-6: Tube with bolt shear out damage

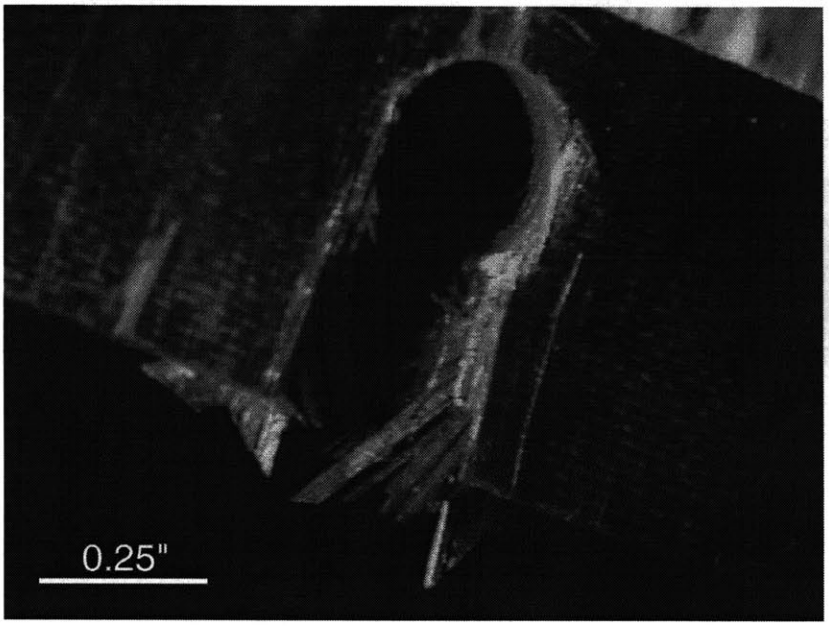

Figure 6-7: Close-up of bolt shear out damage

6.3.2 Aluminum plugs

Sanded

In specimens bonded with film adhesive, failure typically did not occur at the interface between the film and the aluminum in large amounts. One example of limited interfacial failure is shown in Figure 6-8. The sanded aluminum performed well enough that failure was almost entirely interfacial failure between the film and the tube.

Primed

There was minimal adhesive failure between either the film or the epoxy and the aluminum. In joints using primed aluminum with epoxy, the majority of the failure occurred cohesively in the composite.

When primed plugs were bonded with film adhesive, failure was a combination of cohesive failure of the film and of the tube. Primed plugs wrapped in film adhesive often retained graphite-epoxy plies over some region of the bond after pull-out. The size of this region varied from 10% to 50% of the circumference, and up to 2 plies remained attached to the plugs.

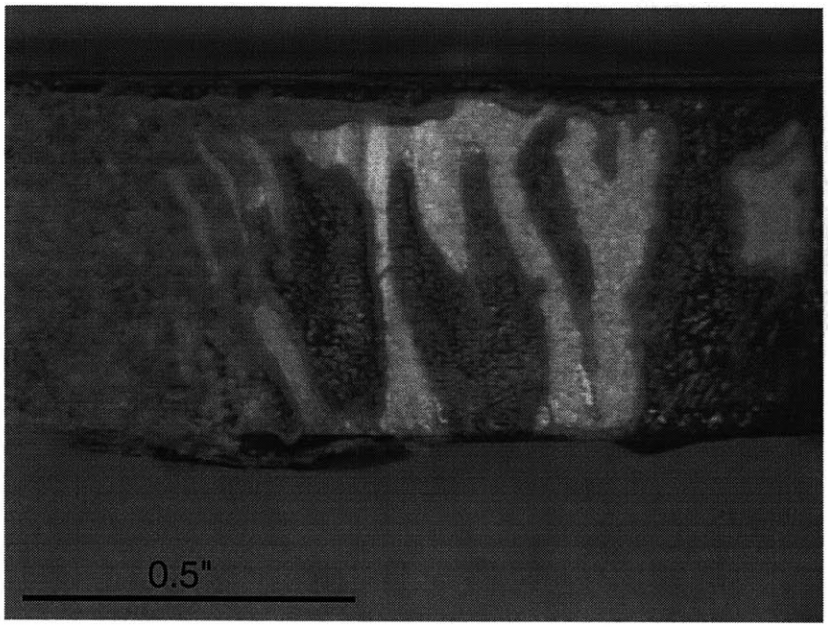

Figure 6-8: Adhesive failure between film and sanded plug

Primed plugs inserted using epoxy broke away less graphite from the tubes, but achieved similar failure loads. Graphite fibers aligned with the 0^o directionwere seen on each epoxy-treated plug after extraction. These fibers were present around the entire surface, but were spread out so the epoxy was visible also. The failed surface somewhat resembled a bar code in this respect.

Tapped

The aluminum plugs which were drilled and tapped to accommodate mechanical fasteners sustained no damage.

6.4 Defects

6.4.1 Eccentricity

The most significant defect in terms of limiting strength was eccentricity of the composite tubes. Since each was slightly elliptical, the spacing between it and the inserted tube varied around the circumference. The effect of this varied depending on the adhesive system used.

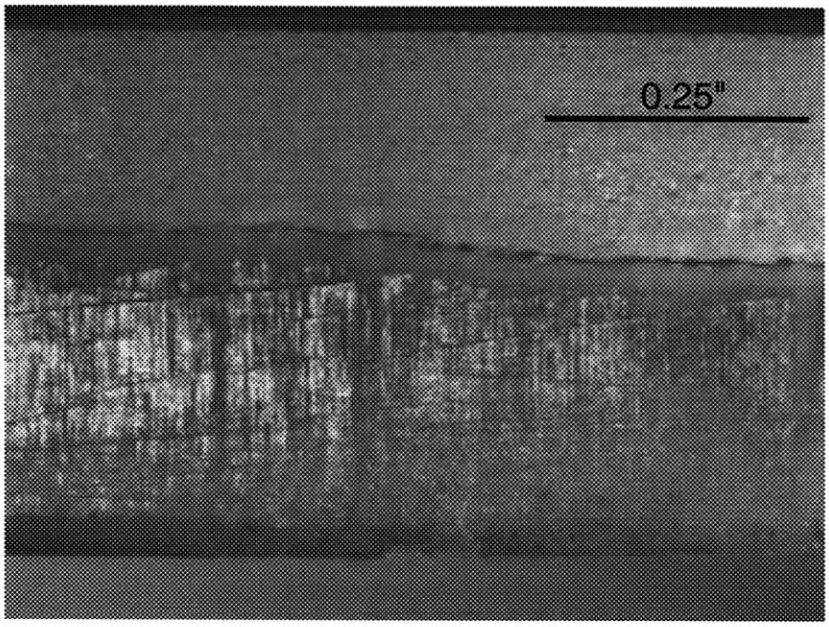

Figure 6-9: Plug with half-thickness epoxy coating

When the specimens were bonded using film adhesive, there were often significant regions (up to 30% of the circumference) which were unbonded after curing. The extent of the unbonded area was determined by observing light leaking between the film and the tube. This inability to bond, despite tight spacing between adherends, is due to the film adhesive not flowing much when curing.

The specimens bonded using epoxy also suffered from the eccentricity. While epoxy does flow much more easily than film adhesive, it cured in these joints such that the regions where the spacing was greatest were only bonded over a portion of the plug thickness. The bond frontier took on a parabolic shape, varying between covering 60% and 100% of the plug thickness. This effect is depicted in Figure 6-9.

In either case, this reduction in effective bonding area may limit the overall strength of the joint, in addition to introducing crack fronts from which to initiate fracture.

6.4.2 Pitting

A byproduct of water jet fabrication of the aluminum plugs was some pitting of the plug surface. This effect was characterized by small hemispherical gouges approximately 0.05" to

0.1" in diameter cut out of the curved surfaces of the aluminum plugs, particularly near the plug edges. Pits were visible over a small area of affected plugs, typically less than 5%.

Since failure at the surface of the aluminum plugs contributed so little to the failure of the joints, pitting is not considered a serious detriment to bond strength.

6.4.3 Surface pores

Epoxy specimens were cured plug-side-down, so that the plug and tube edges would be flush after bonding. Since epoxy was applied liberally to these specimens, the assemblies had a tendency to 'float' on a thin layer of epoxy, which cured to form a shiny epoxy film across the surface. Air bubbles trapped underneath the specimens were manifested as surface pores in this epoxy layer, and considered as defects.

After testing, component surfaces were inspected locally around the pores, but in no case was there evidence that the pores were hazardous to the strength of the bond.

6.5 Displacement

Numerical results indicate the maximum expected extension of the bonded specimens is less than 0.01". Load-displacement plots generated from experiments, however, indicated an approximate displacement of 0.25" per test. An additional test was carried out to characterize the discrepancy.

It was hypothesized that the load-displacement curves generated by experiment reflected the compliant nature of the rubber used in the clamp. The standard test apparatus was installed into the MTS machine, but an unbonded tube was used in place of a complete specimen. The tube was present to constrain the rubber as it had been during the tests. Similarly, a bolt was inserted thru the central hole in the rubber, but was not clasped by the lower MTS grips. Instead, a bolt was installed in the upper MTS grips, and lined up colinearly with the with bolt through the rubber. The lower MTS head was raised, bringing the two boltheads into contact and compressing the rubber. This test generated a load-displacement curve for the rubber in its test configuration. The test setup used to measure

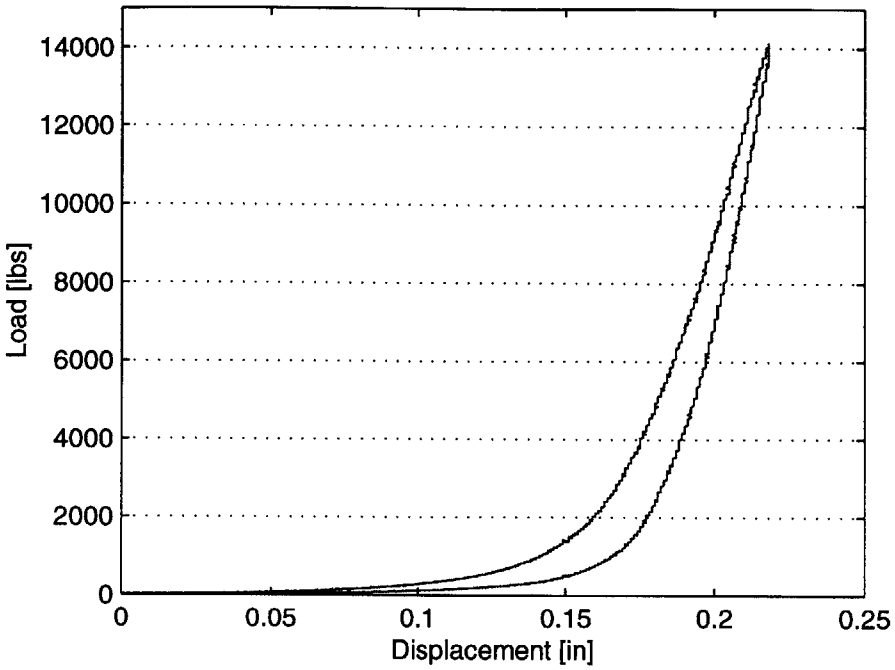

Figure 6-10: Load-displacement curve for 80A rubber plies

the constitutive behavior of the rubber in its test configuration is included as Figure 6.5.

The load-displacement curve for the rubber is shown in Figure 6.5, and superimposed on a typical load-displacement curve obtained during a specimen tensile test in Figure 6.5. The curves match up almost completely, indicating that the recorded displacement data, in the most part, reflected only the rubber. Analytic results indicate that the extension of the test specimen itself (including the bond), is of the order of 0.005", which is comparable to the extension experienced by the steel components of the testing rig, and far smaller than the compression of the rubber. Because of this, the experimental displacement data is not considered to be an accurate indicator of deformation of the test specimens alone.

6.6 Alignment

All critical machining to fabricate the clamping device was completed using a lathe, so that all parts would align coaxially when assembled. The largest allowable error is attributable to the connection between the test specimen and the bolt mounted to the upper MTS grip. This bolt was slightly undersized, at 7/8" diameter, to fit through the 1" hole cut in each

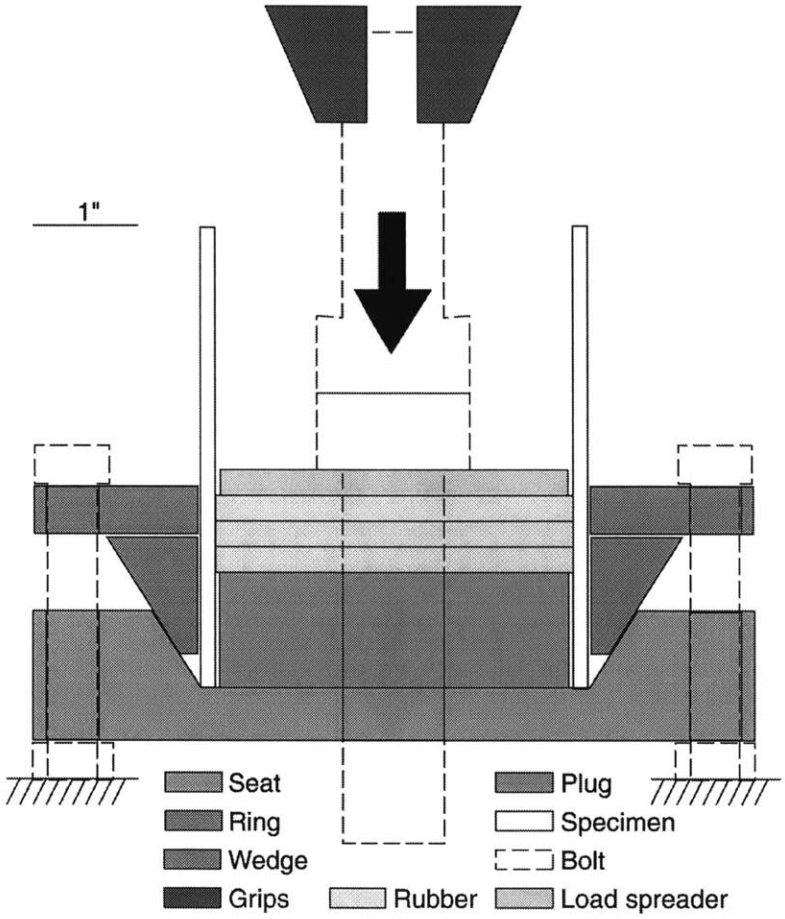

Figure 6-11: Test configuration for determining rubber constitutive behavior

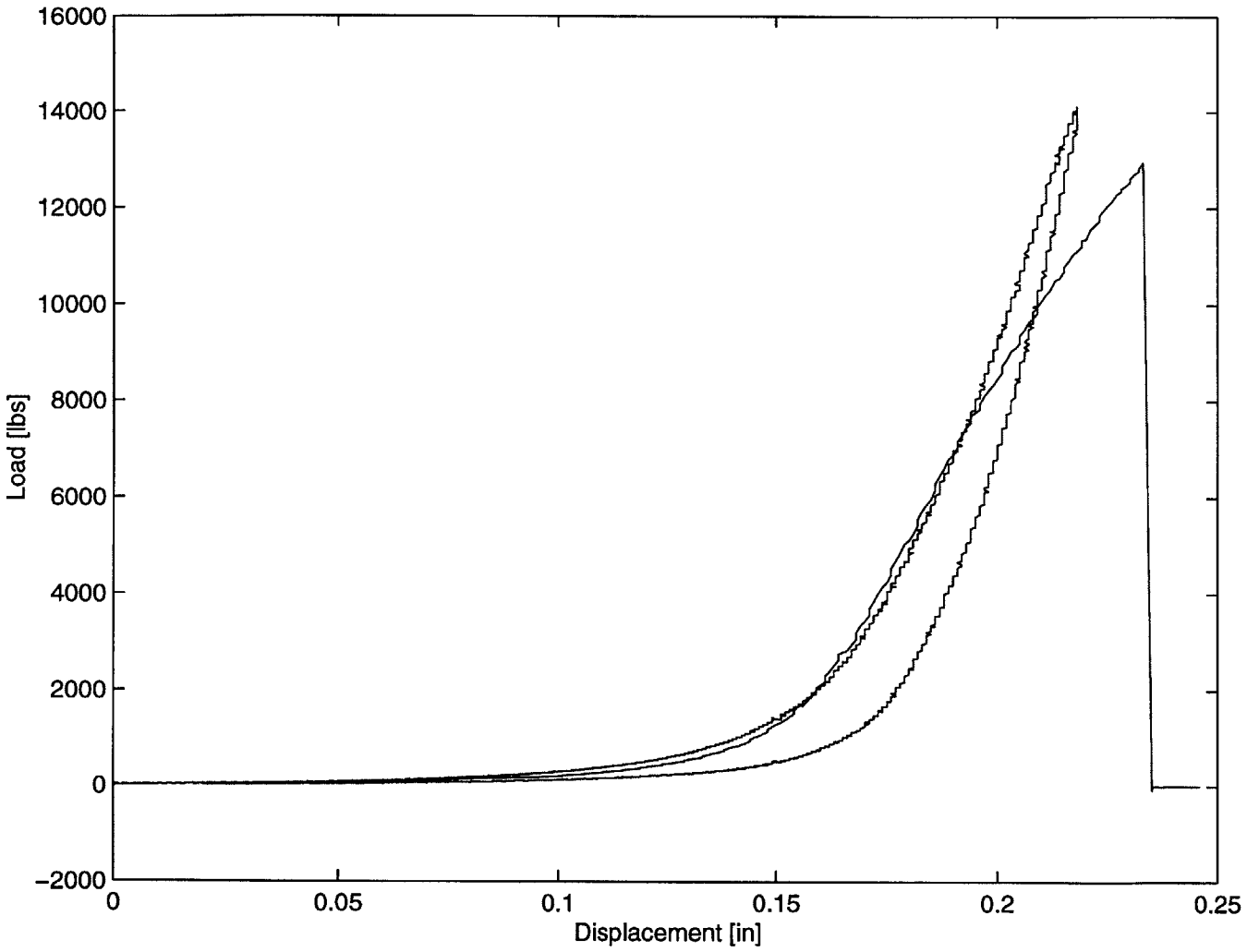

Figure 6-12: Constitutive plot for rubber overlaid on load-displacement curve from tensile test

aluminum disc. As a result, a maximum possible misalignment of the axes was 1/16" in any direction normal to the bolt axis. The bolt was wrapped with rubber tape to increase the diameter uniformly and help seat the bolt centrally through the hole.

The error was also reduced by the self-aligning nature of the MTS grips. The grip pairs used each had a diamond-shaped notch suitable for grasping cylindrical shapes, such as bolts, in a straight, central and vertical orientation. The grips were thus able to align the upper and lower bolts collinearly.

Furthermore, after each specimen was installed in the testing machine, the entire assembly, supported by the two mounting bolts, was rotated by hand about the vertical axis. During this process, the spacing between the upper bolt and the disc hole was observed for variation. This process is estimated to reduce the alignment error further by at least 50%.

The fairly loose spacing between the upper bolt and the disc hole allowed a rotational travel of an extracted plug of approximately 10^o, shown in Figure 6-13. In some tests, The plug was observed to 'pop' out of only one side of the tube, and remain connected on the other side, inclined at this angle. The side of the plug that did not immediately disconnect tended to delaminate the tube due to peel stress created during the sudden rotation of the plug.

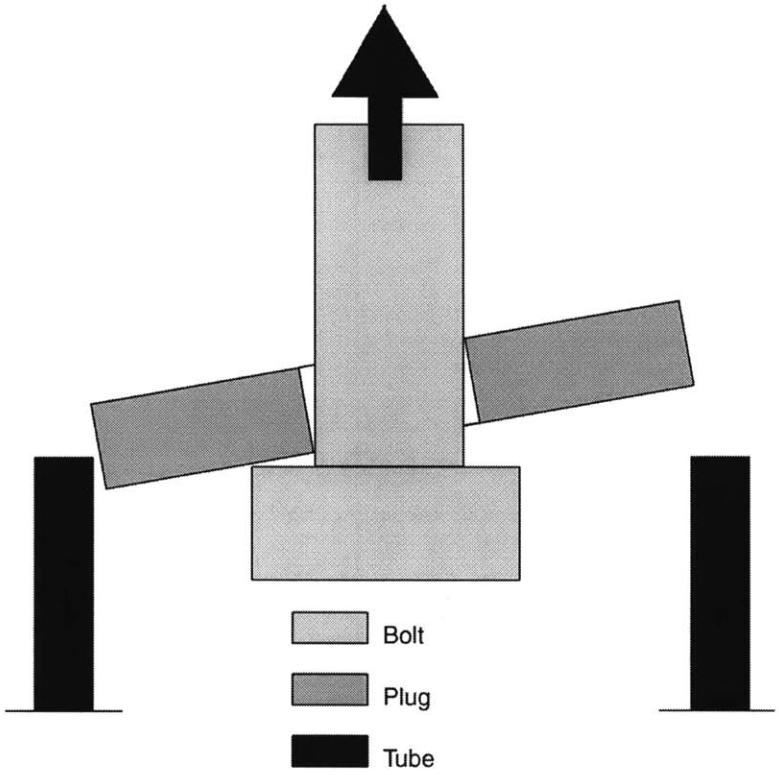

Figure 6-13: Extracted plug at maximum rotation

Chapter 7

Analysis and Discussion

7.1 Effect of surface preparation

The difference in failure modes between the sanded/primed and cleaned/sanded bonded specimens highlighted the importance of proper surface preparation. When the composite tubes were not sanded, adhesive failure between the film and the tube was the major failure mechanism. Failure with cleaned/sanded specimens occured at approximately half of the applied load required for sanded/primed specimens to fail. This illustrates that cohesive failure is preferable to adhesive failure, and shows that sanding the composite tube caused a dramatic increase in bond strength. Since adhesion was largely maintained between the film adhesive and both the sanded and the primed aluminum, conclusions about the importance of aluminum surface preparation in this application could be premature.

7.2 Observed damage

The sanded/primed specimens bonded using film adhesive failed by a combination of cohesive failure in the adhesive and adherend failure of the tubes. These failure types are illustrated in Figure 7-1. The region that failed in the composite was between 10% and 30% of the total bond area. The remaining area was split between cohesive failure of the film, and an unbonded region between the film and the composite. The unbonded region made up

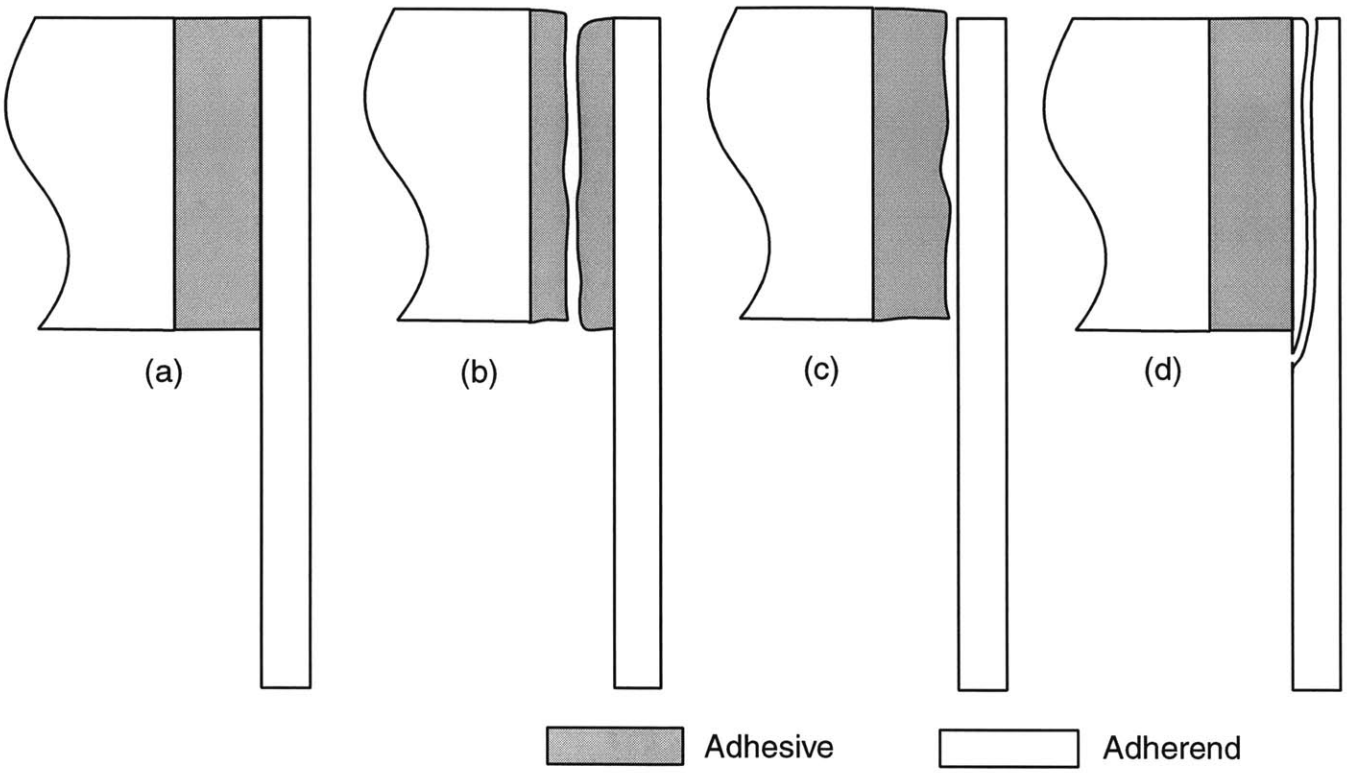

Figure 7-1: Types of bond failure under shear loading. (a) As-cured specimen, (b) cohesive bond failure, (c) adhesive bond failure, (d) adherend failure.

approximately 10% to 30% of the area intended to bond.

In most cases, the appearance of failed film was uniform across the thickness of the aluminum plug. However, in the remaining cases, the film appeared to have failed cohesively at the top edge (which was flush with the tube end), and resembled debonded adhesive at the bottom end. Considering that the film was wrapped down onto the lower planar surface of the plug before insertion, this appearance may indicate that pre-cracks existed at the film/tube interface as a manufacturing by-product. Had fast fracture initiated at those cracks, and proceeded through the adhesive, the observed damage might have resulted.

Analytical results indicate the maximum tensile stress σ_{11} present due to thermal loading occurs at point B (as defined in Chapter 4). Loading the laminate transversely in tension may have caused interlaminar damage between plies near the surface, generating cracks. With sufficient shear loading applied during a mechanical test, fast fracture in mode II could have initiated from such cracks, extending upward to the end of the tube, and inward to its

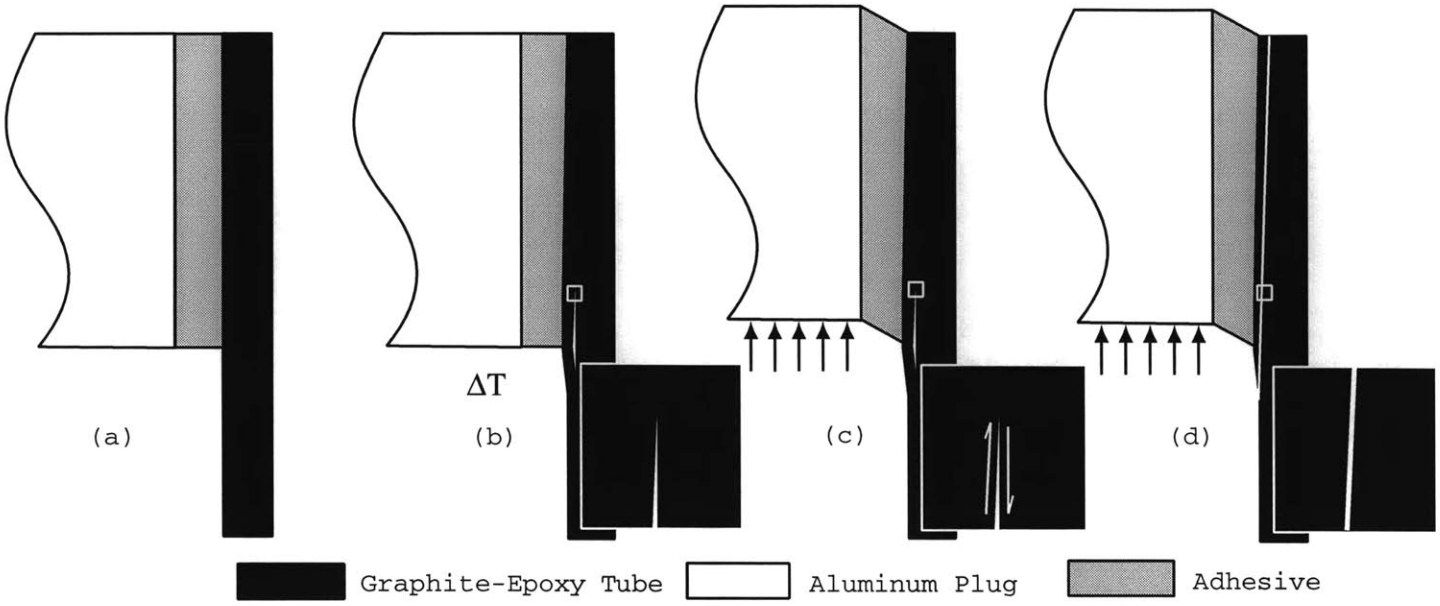

Figure 7-2: Interlaminar fracture scenario in composite tube, proceeding through (a) uncured, (b) cured at temperature, (c) mechanically loaded and (d) post fracture stages.

interior surface. Such a scenario, illustrated in Figure 7-2, would result in macroscopic ply fragments detaching from the tube as were observed in several tests.

7.3 Comparison with flat specimens

Results from Huppe indicate a 500% increase in strength when a sanded/primed preparation is used rather than a cleaned/sanded preparation. For the curved specimens used in this study, the increase in strength using these same preparations was approximately 100%. A number of factors may partially account for this difference.

Firstly, the graphite-epoxy laminates manufactured by Huppe were fabricated using a nylon peel-ply backing sheet applied to each face of the uncured ply stack. These peel plies contain a release agent which allows them to be removed easily from the laminate after curing. However, it was shown by Hart-Smith [29] that the release agent transfers to the cured composite and remains as an unbondable film when the peel-ply has been removed, severly limiting the chemical bonding potential of the surface. Huppe noted that abrading

the composite surface removes the film as large amounts of green powder. The manufacturing process used in this work did not use a nylon peel ply in contact with a bonding surface. Instead, the interior surface of each composite tube, where bonding took place, was layed up directly onto GNPT for curing. The surfaces cured in contact with GNPT were more likely to bond than those in contact with nylon peel-ply.

The absense of adhesive failure between the adhesive and the aluminum seems to indicate that the preparation of the aluminum surface, in this application, may not have been as crucial as in the case of DLS specimens. However, Huppe reported a 20% increase in failure stress using primed/sanded specimens over sanded/sanded specimens, while both experienced adhesive failure in the film.

Huppe reported that the strongest DLS specimens, which used a primed/sanded preparation, underwent yield in the aluminum adherends before failure. Given the geometry and loading for a DLS specimen, this plastic deformation would have relieved stresses in the film adhesive while maintaining the applied load. As a consequence, the strength of the bond increased overall as elastic strain energy in the structure was converted into plastic work done in the aluminum adherends. Due to the thickness and geometry of the aluminum plugs used in this work, the aluminum had no plastic zone and thus the same effect was not realized.

Due to the structural configuration of the test specimens, the adhesive layer was more constrained than in the case of the DLS specimens. Double lap shear test articles are free to contract in their thickness direction due to the effects of poisson's ratio when loaded longitudinally. As the aluminum plug and the composite tube were concentric, and far stiffer than the adhesive layer, the adhesive could only deform in the longitudinal direction under mechanical loading. These constraints increase the stress in the bond compared with a DLS. For the sanded/primed DLS specimens, the ultimate load Huppe recorded was 15% higher than the load at which yield began. Since the aluminum adherend was much thicker than the doublers used by Huppe, failure of the adhesive in the cylindrical specimens was a far more brittle process, and as such did not experience the same strength benefit.

Huppe classified the effect of manufacturing defects on the strength of flat test specimens as 'slight'. The most significant influence of defects was on failure modes. While the sanded/primed DLS articles failed cohesively for the most part, adhesive failure was observed

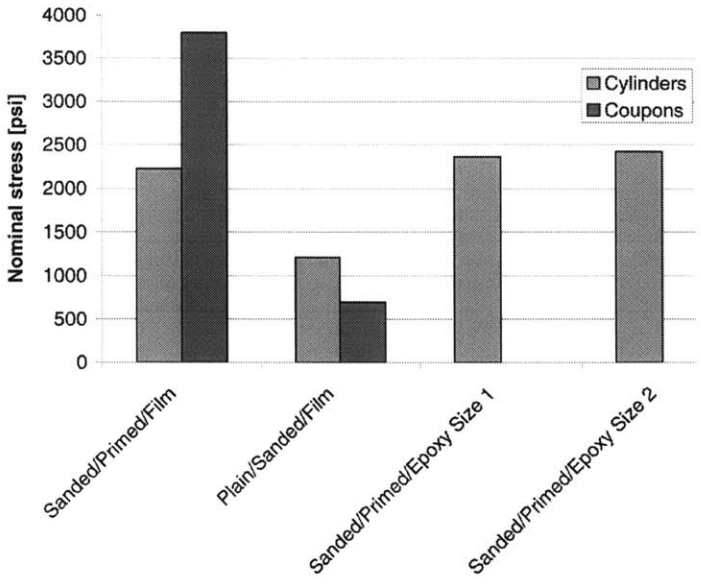

Figure 7-3: Nominal strength of bonded cylinders and DLS specimens

locally where deliberately inadequate surface preparation was performed. In contrast, defects present in the curved specimens tested in this work had a more significant effect. There are a greater number of defect types that can occur with complex, curved specimens than there are for flat specimens like double lap shear articles. In addition to locally-unprepared surface regions on the adherends, there is high sensitivity to misalignment in several axes. Variations in curvature between adherends can introduce insertion difficulties and produce non-uniform bond effects, such as the debonds observed in specimens joined using film adhesive, or the half-bonds observed in liquid epoxy-bonded specimens. These defects in particular can generate cracks from which fast fracture may initiate.

7.4 Empirical-numerical agreement

Figure 7-3 compares the nominal strength of bonded cylinders with that of flat coupons tested by Huppe with the same surface preparations. The nominal strength is obtained by dividing the failure load of the specimens by their bonded area.

The difference in observed strength between the flat and curved specimens indicate that failure stresses obtained from coupon tests are not accurate predictors of the strength of

other structural geometries, when applied in this particular manner. The nominal failure stress of a sanded/primed DLS specimen bonded with FM-123, according to Huppe, is 3800 psi. For comparable cylinders, this figure is only 2230 psi. In contrast, the plain/sanded cylindrical specimens tested in this work had a nominal failure stress of 1212 psi, which is 73% higher than that of the flat coupons, which failed at 700 psi.

7.4.1 Yield

Experimental results indicate that each bonded specimen failed due to fast fracture of the adhesive, of the composite adherend, or at the interface between them. The failure was not consistent with a yield-dominated process. Numerical simulations performed using ABAQUS agree, indicating that the widespread onset of yield according to a Von Mises criterion does not occur until applied loads are well above the failure loads observed. Figure 4-2 indicates that the load-displacement behavior of the bonded specimens remains elastic in the range of interest. Elastic, perfectly-plastic analyses estimate that between 5.2% and 14.3% of the bond material has yielded between 10,500 lbs and 14,000 lbs. In this range, the elastic and plastic load-displacement curves still track very closely.

7.4.2 Fracture

Figure 4-12 shows a linear relationship between applied displacement and stress intensity factor K_{II}, for a given initial crack size, a. Given that the relationship between load and displacement is linear elastic upward of the failure load experienced by the test specimens, this indicates K_{II} is also linear with applied load, P. Incorporating analytical results relating K_{II} to a, the family of curves in Figure 7-4 is constructed. A mode II adhesive fracture toughness of 1500 $lbs/in^{3/2}$ was estimated by multiplying a mode I fracture toughness [2] for a composite-composite adhesive bond by a factor of two. Considering the ratio G_{IIc}/G_{Ic} for adhesives is typically four or greater, and K goes as $\sqrt{G}$, this fracture toughness should give a conservative estimate of critical crack size.

Figure 7-4 shows that K_{II} increases with initial crack size a, indicating that fast fracture will occur at a smaller load when larger cracks are present. The figure further indicates

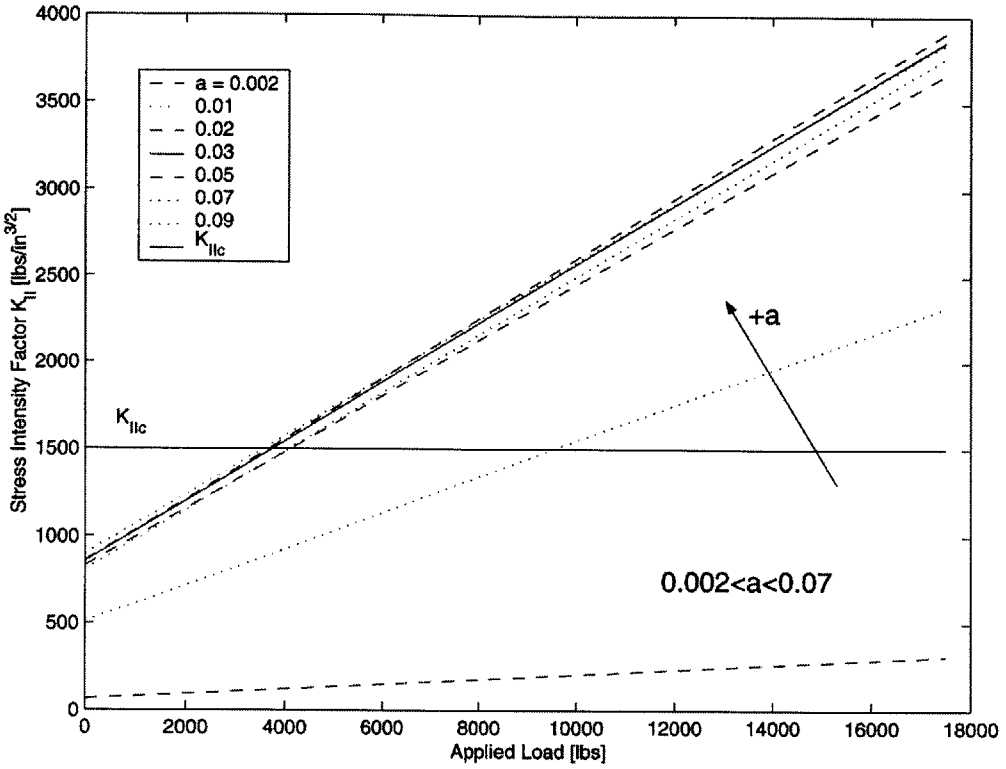

Figure 7-4: Mode II stress intensity factor K_{II} against applied load

that the stress intensity factor increases with initial crack size when only thermal loads are present. Specifying a failure load of 10,000 lbs, it is estimated that fast fracture initiating at the mid-thickness of the adhesive would occur when the initial crack size is 0.01".

Since the location of likely crack initiation was along the bond edge AB, observing defects 3.5" deep, in from the free edge of the tube was difficult. While debonds could be detected due to visible light passing between the adherends, cracks within the adhesive were not detected. However, with the film adhesive folded down onto the upper and lower surfaces of the plug, the presence of interface cracks on this order could be inferred from the geometry, as illustrated in Figure 7-5.

7.4.3 Deformation

Load-displacement data obtained experimentally shows that loads were increased steadily over crosshead travel of approximately 0.25". However, analytical results suggest that an equivalent load should be applied via a specimen extension of approximately 0.005". Addi-

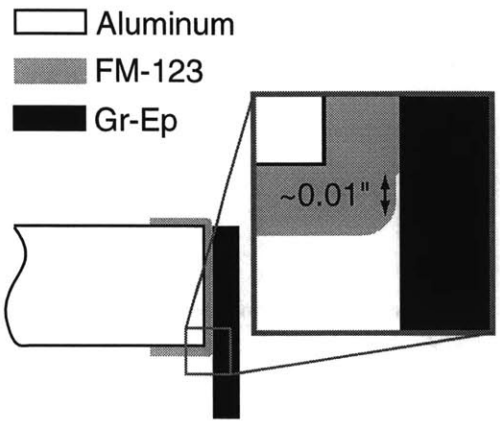

Figure 7-5: Interface crack introduced by film wrapping

tional testing has shown that this discrepancy is due to appreciable compression of the rubber inserts used to clamp each test specimen. The constitutive behavior of the rubber exactly matches the load-displacement data recorded during the mechanical tests. By subtracting the deformation of the rubber from the recorded displacement data, only small displacements remain. While the testing machine is capable of displacement resolution of this order, variations in the behavior of the rubber from test to test preclude accurate measurement of the specimen deformation.

7.4.4 Unquantified factors

Multiple failure modes

Specimens failed by a combination of modes, in most cases. The strongest film adhesive specimens exhibited evidence of cohesive failure in the film, as well as varying amounts of adherend failure of the composite laminate. The liquid epoxy-covered plugs appeared to retain a superficial layer of fibrous material after extraction. The relative extent of each type of failure would ultimately determine the overall strength of the structure. The major causes of failure appear to have been fracture within the adhesive, interfacial fracture between the adhesive and the composite, and interfacial fracture between plies of the tubular laminates. The thermally and mechanically introduced stresses responsible for each of these have been the modeling focus.

Defects

The presence of numerous types of defects have a bearing upon the experimental outcomes and the strength achievable by these specimens. The majority of observed defects (surface pores, pitting) did not appear to have an influence out of balance with their limited occurences over small regions. Larger defects, such as the debonds observed in film adhesive specimens, may have had a more considerable limiting effect on joint strength. However, inspection of extracted aluminum plugs with a film adhesive coating reveal this debond effect to be wholly present throughout the batches of film adhered specimens. One could estimate that the strength of the bond is reduced by the same factor as is the effective area, when these debonds are present. However, this could not be confirmed as no uniformly bonded specimens were successfully assembled.

Material properties

The prepreg material used to fabricate the composite cylinders was older than the shelf life recommended by the vendor. The film adhesive was also significantly aged. Their age may have degraded the cured properties of both materials. For this application, the most sensitive variations would likely be the shear strength of the adhesive and the interlaminar shear strength of the graphite-epoxy laminate. Work by Watkins and Park [3] proceeded Huppe by approximately 6 months, using the same batch of film adhesive. This film was used again approximately 4 months later for this project. Watkins and Park noted that their specimens exhibited lower strengths than those tested by Huppe, and suggested age-related degradation of the film adhesive may have been a factor.

Chapter 8

Conclusion

High reliability joining of curved structures is realizable. With proper surface preparation of adherends, small standard deviations in failure load are achievable. The coefficient of variation of failure load for the sanded/primed specimens was less than 0.06, and in the case of the liquid epoxy specimens, it was smaller than 0.03.

Mechanical fastening has little potential when joining near laminate edges. Shear out failure dominates over other bolted failure modes when screws are positioned close to the ends of the tubes. With additional screws, failure loads can be increased, but in order to achieve comparable strength to an adhesive bond, the screws would be so numerous as to suffer net-tension failure from being placed to close together. In addition, an aerospace vehicle with a composite fuselage would likely use countersunk fasteners to reduce drag, which might create more extensive damage to the composite, and further reduce the strength of the bond.

8.1 Recommended manufacturing procedures

Aluminum components should be etched and primed to promote maximum adhesion between the metal and whichever adhesive system is used. Maximum adhesion to polymer composites with thermosetting matrices is achievable by abrading the surface of the composite laminate.

When bonding inserts using film adhesive, sufficient clearance must be allowed between the adherends for the thickness of the adhesive, plus an allowance for the tackiness of the

film. If the clearance is too small, the film will be scraped off the plug by the tube during insertion. To keep the film from bunching up as the plug is inserted, it is recommended that the film be cut oversized, and applied with excess film extending along the thickness axis in both directions. Folding this excess down onto the flat surfaces of the plug increases the friction between the film and the metal, which holds the adhesive in place during insertion.

Since film adhesive flows minimally, it is important to minimize the clearance between the adherends, beyond that required to fit the film in between them. Eccentricity in either adherend causes variation in clearance around the circumference of the structure, and can result in unsuccessful bonding in regions where the spacing is greatest.

The film adhesive should be cured at the recommended temperature, but a hyperbaric chamber or autoclave is neither necessary nor particularly able to exert pressure on the bond. The adhesive lies between two quite stiff adherends, which are incapable of transferring hydrostatic air pressure to the bond. Rather, the appreciable thermal expansion of the aluminum when raised to the cure temperature exerts pressure on the film, while the composite tube remains almost thermally inert.

Bonding using liquid epoxies makes the insertion process easier, because they are able to flow and fill in any gaps between the adherends. The excess epoxy also tends to center the plug in the tube by 'floating' it into a position where the epoxy is in equilibrium. The eccentricity of the tubes can also reduce bonding effectiveness in regions where the spacing between the adherends is greatest. However, since the epoxy can flow freely, the effect is different than encountered with film adhesive. Rather than regions remaining wholly unbonded, they bond only partially in the thickness direction of the plug. This effect is reduced by applying epoxy liberally to both adherends, rather than just the plug. Having both surfaces wetted before insertion reduces the tendency for epoxy to flow away from regions with wider spacing.

The additional benefit of using epoxies that can be cured at room temperature is that residual stresses are not introduced. Cooling down a specimen bonded with film adhesive from its cure temperature to room temperature introduces stresses into the film caused by thermal mismatch between the components of the bond. An epoxy bond which is stress free at room temperature possesses a higher potential for strength than a film cured at elevated

temperature, assuming the epoxy system is intrinsically as strong as a film adhesive.

Manufacturing fastened joints is not recommended for tensile tests near laminate edges, due to the susceptibility of such joints to shear out failure of the fasteners. Increasing the number of fasteners to improve the load-capacity of the structure introduces the risk of net tension failure of the joint as screws are placed in closer proximity. By scaling the diameter of this structure, more screws could be accommodated before net tension dominates, but in doing so the bondable area would also scale, the load capacity of a bonded joint would grow at the same rate as would the bolted joint.

8.2 Recommended testing procedures

A significant part of the peripheral work completed in pursuit of this thesis was the design and fabrication of a testing fixture, capable of constraining the specimens under significant loading. A number of design iterations were necessary to construct an apparatus that functioned satisfactorily. In light of testing difficulties encountered, experimental recommendations are included here.

A clamping device for cylindrical structures is described in Chapter 5. This device was an effective interface between the grips of the servohydraulic testing machine and the tubular specimens. Under certain easily encountered circumstances, the setup was much reduced in its capabilities.

The greatest obstacle to a successful test to failure is slippage of the specimen out of the clamp. The final design iteration incorporates eight 7/16" bolt holes spaced at 45^o intervals around the circumference of the clamp. The bolts need to be tightened in opposing pairs, and tightened gradually so that the clamp parts remain in parallel planes. If one side is tightened preferentially, the maximum clamping effort can not be effected. Loosening of the clamp after a test should follow the same procedure to prevent damage to the bolts.

Positioning of the specimen is also critical for even loading and accurate data. To ensure the specimens seat completely in the clamp, it is recommended that the wedge ring be slid up around the specimen so that there is approximately 1/4" spacing between the bottom edge of the wedge and the bottom edge of the tube. That way, as the clamp is tightened

together, the wedge will be driven down into the seat, and will pull the tube into position also. Any more than 1/4" spacing and the bolts may not extend far enough through the bolt holes to attach nuts and begin tightening.

Once fully installed into the test fixture, a specimen should be marked so that slippage out of the clamp can be detected promptly. A strip of masking tape applied to the tube, level with the topmost part of the clamp at eye-level is a good indicator.

With the testing apparatus in place in between the grips of the MTS machine, alignment of the fixture can be visually inspected. The test fixture is free to turn about its axis, and doing so will show any eccentricity of the mounting.

In light of the load levels used when testing, a plexiglass shield should be used to protect anyone near the testing machine. The nature of the failure of the joints is such that there are usually no fragments or other loose debris following a test, but the clamp, which is heavy, will fall back onto the MTS actuator at failure, so hands should be kept clear until a test is concluded.

After uninstallation of the fixture from the test machine, the broken specimen should be inspected and documented before removal from the clamping device. The removal procedure can be time-consuming and inadvertant damage to specimens may occur while it is being carried out.

8.3 Recommended modeling procedures

Given the presence of the aluminum plug, the size of the model is quite large compared with the area of interest for analyzing the joint. The small region comprising the adhesive itself and the material around it requires a high resolution mesh of finite elements to estimate accurately the mechanics of that region. To limit the computing power required to invert the stiffness matrix for the structure, the mesh should remain coarse in regions sufficiently far from the bond. The interior region of the aluminum plug and the unbonded end of the tube experience only small gradients in stress, and no plasticity. The coarse and fine meshes must remain compatible to yield valid results. In this work, the coarse meshes were constructed from high aspect ratio elements. Nodes would be spaced close together in one direction, but

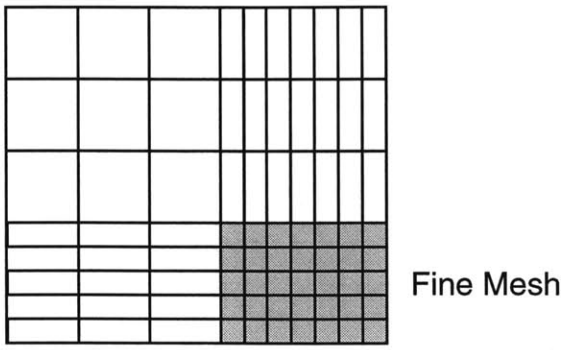

Figure 8-1: Compatible coarse-fine mesh

farther apart in the orthogonal direction. A compatible fine mesh region could be interfaced with these elements by simply shortening the node spacing in both directions. A short-x by long-y strip of elements intersecting a long-x by short-y strip of elements creates a short-x by short-y grid, as well as a long-x by long-y element grid, as shown in Figure 8-1.

The most sensitive region of the bond lies near point B (as defined in Chapter 4. Downward from this point, all of the applied load is transferred through the thin composite tube. Upward from B, this load is spread over a much greater area, so the stress gradients in this region are quite large.

Modeling difficulties were encountered when significantly thinner adhesive layers were incorporated into the model. Elements underwent significant deformation, producing questionable results, and a converged solution was often difficult to obtain. For significantly thinner adhesive layers, alternate modeling methods should be explored.

Solutions obtained from FRANC for fracture analysis were very sensitive to mesh construction. Despite the active remeshing capability of the software, which partially deletes the user-defined mesh around a pre-crack and constructs its own mesh, the new mesh must be made compatible with the remainder of the user-defined mesh. If crack locations specified by the user are near the boundary between a coarse and fine mesh, the reconstructed mesh may include poorly-shaped elements to join up with distant nodes in the coarse mesh. Cracks should only be initiated in locations where the mesh geometry is uniform for several characteristic lengths all around the pre-crack. For the edge cracks generated for this work, it was sufficient to have the bond material finely meshed, with the adherends less so. This

gave consistent estimates of K_{II} between the different calculation methods FRANC uses. For additional work, perhaps focused on interface cracks, the fine mesh should be extended well into the adherend so that the reconstructed mesh is well-shaped.

8.4 Applicability of coupon data

Mechanical behavior of complex structures can not be predicted easily based upon behavior of simple structures intended for determining material properties. It has been shown that bond strength cannot be accurately predicted by simply multiplying the failure stress of a flat specimen by a ratio of bonded areas. The differences in geometry have many implications for strength, and for each geometry these implications will be different.

The cylindrical specimens used for this work have been shown to vary from their flat counterparts in loading, stress state, constraints on deformation, adherend ductility, thermal response and defect sensitivity. While these curved specimens experienced a similarly applied load to flat double lap shear articles, biaxial thermal stresses present in the adhesive reduced the load-carrying capacity more than the uniaxial thermal stresses present in DLS specimens, due to additional constraints imposed by the structural geometry.

The structural geometry again, exerts a significant influence on the failure modes observed during testing. Deformation constraints caused by comparatively thick and stiff adherends, particularly ones held coaxially, bring about a more brittle failure process than occurs with thin metal adherends such as DLS doublers. Such ductile structures, which fail after significant plastic adherend deformation, naturally exhibit higher ultimate stresses than are seen with larger adherends which barely deform before joint failure.

It is possible to construct models of generic bonded structures, calibrated using material data obtained from coupon tests, which account for these additional complexities. It should be recognized that the load-carrying capacity of a bonded structure does not adequately describe its complete stress state when large temperature changes occur after bonding. A stress state calculated in consideration of both thermally and mechanically-induced stresses can be used to predict the onset of plasticity, and to estimate the stress intensity factor around an assumed crack tip.

For an adhesive bond, maximum joint strength is achieved under adherend failure. Cohesive failure of the adhesive layer is secondarily desired. If either occurs, it indicates that the adherend surfaces have been adequately prepared to maintain a chemical bond to the adhesive material. Experimental results of DLS tests have shown the strongest bonds were achieved by sanding composite adherends and chemically etching and priming aluminum adherends before bonding. These preparations were shown in this work to provide a significant strength improvement, approximately 100%, over a plain/sanded preparation. While the strength improvement is not as significant for cylindrical specimens as for flat coupons, the effect of foregoing adhesive failure in favor of primarily cohesive failure at a far higher load is the same.

8.5 Future work

Additional investigation into bonding curved structures should explore the effects of a number of different factors, in order to expand the design space of generic curved structures. It has been shown [11] that performance benefits demonstrated using flat coupons offer different magnitudes of improvement when applied to particular structures. A cost-benefit analysis done to identify other sensitivities to geometry could be useful.

Comparable tests to those presented here, using adherends with particular defects near the bonded region, could provide valuable insight into structural succeptability to to production flaws. Specifically, incorporation of pre-cracks into the bond or at the bond interface could support the creation of a more detailed fracture model of this geometry.

The influence of edge effects for specimens similar to these could be investigated by conducting compression tests to push the plug deeper into the tube rather than pulling it out. It is anticipated that such tests would be experimentally much more straightforward, since overcoming slippage of the specimens would not be an issue.

The general absence of adhesive failure between the film and the sanded aluminum calls into question the necessity for priming the aluminum. A few extra tests of a sanded/sanded preparation using film adhesive would illuminate this matter.

Bibliography

[1] Gosse, J. H. and S. Christensen, "Strain Invariant Failure Criteria for Polymers in Composite Materials," Tech. Rep. AIAA-2001-1184, American Institute of Aeronautics and Astronautics, 2001.

[2] Huppe, B. A., *High Reliability Adhesive Joining of Metal and Composite Components*, Master's thesis, Massachusetts Institute of Technology, June 2001.

[3] Park, M. and R. Watkins, "The Effects of Thermal Environment on Adhesive Metal-Composite Joints," tech. rep., Massachusetts Institute of Technology, December 2001.

[4] Sotiropoulos, S., H. V. S. GangaRao, and R. Lopez-Anido, "Evaluation of FRP Composites Bolted and Adhesive Joints," in *Materials for the new millenium: proceedings of the Fourth Materials Engineering Conference* (Chong, K. P., ed.), Materials Engineering Division of the American Society of Civil Engineers, November 1996.

[5] McMaster-Carr, "Physical and Mechanical Properties of Aluminum Alloys." Document 8975KAC.

[6] Herakovich, C. T., *Mechanics of Fibrous Composites*, John Wiley and Sons, Inc, 1998.

[7] "CytecFiberite Selector Guide," 1998.

[8] Kessler, S. S., *Design and Manufacture of a High-G Unmanned Aerial Vehicle Structure*, Master's thesis, Massachusetts Institute of Technology, February 2000.

[9] Andrews, D. R., ed., *Soldering, Brazing, Welding and Adhesives*, The Institution of Production Engineers, 1978.

[10] Hoskin, B. and A. Baker, eds., *Composite Materials for Aircraft Structures*, AIAA Education Series, American Institute of Aeronautics and Astronautics, 1986.

[11] Davis, M. and D. Bond, "Principles and practices of adhesive bonded structural joints and repairs," *International Journal of Adhesion & Adhesives*, Vol. 19, 1999, pp. 91–105.

[12] van Rijn, L. P. V. M., "Towards the fastenerless composite design," *Composites Part A*, Vol. 27A, 1996, pp. 915–920.

[13] Chamis, C. C. and P. L. N. Murthy, "Simplified Procedures for Designing Adhesively Bonded Composite Joints," *Journal of Reinfoced Plastics and Composites*, Vol. 10, January 1991, pp. 29–41.

[14] Hart-Smith, L. J., "Analysis and Design of Advanced Composite Bonded Joints," Tech. Rep. NASA CR-2218, NASA, August 1974.

[15] Ratwani, M. M. and H. P. Kan, "Analysis of Composite-to-Metal Joints with Bondline Flaws," *Composites Science and Technology*, Vol. 23, 1985, pp. 53–72.

[16] Loftus, D., M. S. Found, and J. Yates, "The performance of aluminium to carbon fibre composite bonded joints in motorsport applications," *Sports Engineering*, Vol. 2, 1999, pp. 235–243.

[17] Shetty, S. P. and S. M. Spearing, "The Reliability of Composite-Metal Adhesive Joints Subject to Thermo-Mechanical Loading," in *AIAA/ASME/ASCE/AHS/ASC Structures, Structural Dynamics, and Materials Conference and Exhibit, 38th, and AIAA/ASME/AHS Adaptive Structures Forum, AIAA-97-1222*, 1997.

[18] Janardhana, M. N., K. C. Brown, R. Jones, and J. Paul, "Effect of Debonding on Adhesively Bonded Composite to Metal Joints in Compression," *Composite Structures*, Vol. 5, 1986, pp. 1–14.

[19] Carter, A. B. III, "Adhesive Bonded Fasteners, A "No Holes" Solution For Space Vehicle Construction," in *30th International SAMPE Technical Conference*, 1998.

[20] Higgins, A., "Adhesive bonding of aircraft structures," *International Journal of Adhesion and Adhesives*, Vol. 20, 2000, pp. 367–376.

[21] Mortensen, F. and O. T. Thomsen, "Coupling effects in adhesive bonded joints," *Composite Structures*, Vol. 56, 2002, pp. 165–174.

[22] Thouless, M. D., J. L. Adams, and M. S. Kafkalidis, "Determining the toughness of plastically deforming joints," *Journal of Materials Science*, Vol. 33, 1998, pp. 189–197.

[23] Hart-Smith, L. J., "Adhesive-Bonded Double-Lap Joints," Tech. Rep. NASA CR-112235, NASA, 1973.

[24] Ashby, M. F. and D. R. H. Jones, *Engineering Materials 1: An introduction to their properties and applications*, Butterworth-Heinemann, second edition ed., 1996.

[25] Wawrzynek, P. and A. Ingraffea, *FRANC2D: A Two Dimensional Crack Propagation Simulator, User's Guide*, version 2.7 ed., 1993.

[26] Gibson, R. F., *Principles of Composite Material Mechanics*, McGraw-Hill, 1994.

[27] Anderson, T., *Fracture Mechanics: Fundamentals and Applications*, CRC Press, LLC, 1995.

[28] Shih, C., A. de Lorenzi, and M. German, "Crack extension modeling with quadratic isoparametric elements," *International Journal of Fracture*, Vol. 12, 1976, pp. 647–651.

[29] Hart-Smith, L. J., G. Redmond, and M. J. Davis, "The Curse of Nylon Peel Ply," in *41st International SAMPE Symposium*, 1996.